

Chapter 14

A Review of Residential-Scale Natural Gas-Powered Micro-Combined Heat and Power Engine Systems



Gokul Vishwanathan, Julian Sculley, David Tew and Ji-Cheng Zhao

Abstract A combined heat and power (CHP) system typically employs a prime mover generator that produces electricity on-site and utilizes waste heat energy to supplement a site's thermal load requirements. Micro-CHP, notionally defined as CHP systems with a capacity lower than 50 kW, offers an alternative, and in some cases a complementary, solution to centralized power generation. A micro-CHP system would be typically installed at a residential or small commercial site where it would consume fuel such as diesel or natural gas to generate electricity locally and further use the rejected waste heat for local heating, air-conditioning, and/or humidification needs. This is in contrast to the rejected heat being dissipated at centralized power plants using cooling towers. The combined efficiency of primary energy usage for such systems can be higher than 90% on a fuel lower heating value (LHV) basis. Since a large fraction of the electricity generated from all the centralized power plants is consumed by the residential and commercial sectors, CHP implementation in these sectors can have a huge impact on both energy savings and carbon dioxide (CO₂) emissions' reduction. Apart from these benefits, decentralized CHP as a form of distributed electricity generation offers numerous advantages such as reduced electrical grid stress, reduced electricity transmission and distribution losses, and potentially improved resiliency of the electricity grid. Various technologies including reciprocating internal combustion engines, Stirling engines, Brayton cycle engines, Rankine cycle engines, fuel cells, and solid-state devices such as thermoelectric generators and thermionic generators can be used as

G. Vishwanathan (✉) · J. Sculley
Booz Allen Hamilton, Washington, DC 20005, USA
e-mail: vishwanathan_gokul@bah.com

D. Tew · J.-C. Zhao
Department of Energy, Advanced Research Projects Agency-Energy (ARPA-E)
United States, Washington, DC 20585, USA

J.-C. Zhao
Department of Materials Science and Engineering, The Ohio State University,
Columbus, OH 43210, USA

micro-CHP systems. This chapter provides a detailed technological review of engine-based micro-CHP systems and further presents the challenges and opportunities for achieving high fuel conversion efficiency.

Keywords Combined heat and power • Internal combustion engines
Stirling engines • Brayton cycle engines • Micro-cogeneration • Micro-CHP
Natural gas generators • Distributed generation

14.1 Introduction

Micro-combined heat and power (CHP) systems have the potential to reduce the energy and emissions burdens associated with the provision of electricity, heat, and cooling services to our homes and small businesses. They also have the potential to enhance the reliability of the electricity supplies of their owners through their redundancy with the electric grid. However, the societal-level energy, emissions, and reliability value propositions that these systems could offer through their widespread deployment are currently at risk due to the high installed costs of these systems versus the energy cost savings benefits that they generally offer. This chapter offers a review of the state of the art of micro-CHP systems for residential applications and discusses several ongoing development programs that are seeking to enhance their energy and economic value propositions and thereby enable their widespread market adoption and the realization of the society-level energy, emission, economic, and reliability value propositions that they can offer.

CHP systems offer their energy, emissions, and reliability value propositions via their on-site generation of electric power and subsequent productive utilization of waste heat from the generation process for local space and/or water conditioning purposes. These systems (typically) convert the heating value of natural gas into electricity and useful thermal energy and can do so at combined overall (i.e. electricity + thermal energy) lower heating value (LHV) basis efficiencies that are in excess of 90%. This efficiency is well in excess of the average 2017 US central plant electricity generation efficiency of 33.6% (Energy Flow Charts 2018). Furthermore, a large (>60%) percentage of US utility-generated electricity is generated from fossil fuels, and the associated CO₂ emissions were 2 billion metric tons of CO₂ in 2014, which was roughly 38% of total US CO₂ emissions (Carbon Flow Charts 2018). Consequently, the widespread deployment of CHP systems across the residential and commercial sectors could have significant primary energy usage and CO₂ emissions reduction benefits, since a combined 74% of the electricity generated by centralized power plants is consumed by these sectors (Energy Flow Charts 2018).

However, despite these potential benefits, less than 500 of the 58.6 million US homes with natural gas have installed micro-CHP systems (EIA 2018; Guyer 2015). The best-performing small-scale CHP engine (~1.2 kW electrical power) has a fuel-to-electrical conversion efficiency of about 26.3% (based on fuel LHV) and a

total CHP efficiency of 92% (Honda Worldwide|Power Products 2018), but the estimated installed cost is more than \$10,000. This system is sufficient to supply the base electric load of many residences, and hence, these residences would be independent of grid electricity during off-peak periods. Tapia-Ahumada et al. (2013) performed a detailed sensitivity study of the penetration of CHP technologies over a 20-year time frame as a function of micro-CHP capital cost (product cost and not installed cost¹). It can be inferred from their study that CHP systems can have a significant impact on the residential sector only when the capital cost is less than \$4,000 per kW of electricity generation. Beyond this value, the market penetration shrinks significantly as the economics of the system becomes unattractive to potential residential customers.

A recent study by the authors (Vishwanathan et al. 2018) assessed the value proposition of residential CHP in the USA. The study selected a few cities from the seven Building America Climate Zones (2018) and calculated customer payback periods using a variety of scenarios that perturbed the technical parameters of a hypothetical residential CHP system installed in a 2,500 sq. ft. single-family home. The baseline scenario assumed a variable fuel-to-electrical conversion efficiency with respect to the electrical load and a peak efficiency of 40%. The total CHP efficiency (sum of fuel-to-electrical conversion efficiency and thermal efficiency) was assumed to be 80%. It was assumed that the 1-kW system followed the residential electrical load and had a total installed cost of \$4,500. The conclusions from this study were that the tradeoffs between system size, cost, and efficiency are extremely important in developing the right product for each climate zone. The baseline scenario showed that it was possible to achieve a payback of less than 10 years in regions where the spark spread² was high (e.g. Los Angeles) or in cold climates where there was significant need for heating throughout most of the year (e.g. Boston, Denver, and Chicago), as illustrated in Fig. 14.1 (Vishwanathan et al. 2018). Finally, it was concluded that a maximum primary energy saving of 0.6 quadrillion BTU in the USA can be achieved with a total installed system cost of \$2,500.

Thus far, micro-CHP technologies have had substantially greater market success in Japan and somewhat better success in the European Union (especially Germany) (Ashurst 2016). Specifically, while the USA can claim 500 residential micro-CHP systems, roughly 50,000 units were installed in Japan in 2015 alone and Germany accounts for over 80% of the micro-CHP sales in the European Union. The enhanced market penetration in Europe and Asia is driven at least in part by supporting government policies and incentives—including net metering, tax incentives, up-front grants, subsidized natural gas (NG) prices, and favorable tariff structures. Barbieri et al. (2012) concluded that the marginal cost for a micro-CHP

¹The gross installed cost of the CHP system includes the product cost and system installation cost.

²According to the US Energy Information Administration (EIA) Web site, spark spread is defined as “the difference between the price received by a generator for electricity produced and the cost of the natural gas needed to produce that electricity.”

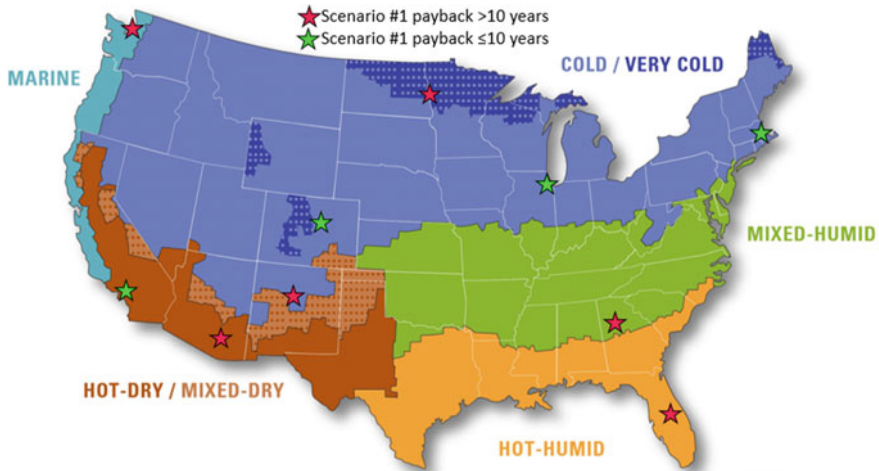


Fig. 14.1 Customer payback analysis performed for ten cities in seven climate zones in the USA (Vishwanathan et al. 2018)

system, with respect to a traditional boiler, must be $\sim 3,000$ €/kW for the system to be economically attractive in Italy. In their study, it is assumed that traditional household boilers will be replaced by micro-CHP systems. Their analysis evaluated a number of potential micro-CHP system technologies and predicted a $> 20\%$ primary energy savings in two single-family home scenarios for Italy. They furthermore concluded that Stirling engine micro-CHP systems provided the most potential energy cost savings. Fubara et al. (2014) performed a mathematical modeling and optimization study at the building level and the overall energy supply network level for NG-fueled micro-CHP systems employing solid oxide fuel cells (SOFC), Stirling engines, and internal combustion engines (ICEs). At the building level, the micro-CHP system was connected to the external gas and electric networks and served the needs of the building. The overall energy supply network simulations included gas production assets, power stations, gas and electricity distribution networks, and building-level domestic energy users. A detailed case study for the UK domestic energy supply was performed for four different residential house sizes for a) cost-driven strategy, obtained by maximizing net present value, and b) primary energy-driven strategy, obtained by maximizing savings in primary energy consumption. A 3–6% reduction in primary energy (NG) consumption was estimated with the cost-driven strategy with SOFC micro-CHP systems, while a 6–10% reduction in primary energy (NG) consumption was estimated with the primary energy-driven strategy with Stirling engine micro-CHP systems.

Ren and Gao (2010) performed an economic and environmental evaluation of micro-CHP systems for residential buildings in Japan. In their analysis, they considered both a 1-kW NG engine and a 1-kW fuel cell system that were optimized to operate for (a) minimum annual energy cost and (b) minimum CO₂ emissions. The

fuel-to-electrical conversion efficiencies of the gas engine and the fuel cell were assumed to be 20 and 37%, respectively. When the systems were operated for minimum annual energy cost, the gas engine resulted in 24% savings while the fuel cell resulted in 26% savings. When the systems were operated with an eye on maximizing the environmental benefit, the gas engine resulted in a 2% reduction in CO₂ emissions while the fuel cell resulted in a 9% reduction in CO₂ emissions. Thus, their analysis showed that fuel cell systems were more effective than the NG engines from both an economic and environmental standpoint.

Given that there is a general consensus that micro-CHP can lead to economic and energy savings, this chapter is dedicated to the review and analysis of NG-powered micro-CHP engine systems. This chapter is organized into two main sections. Section 14.2 presents a detailed review of small-scale engines that are relevant to residential CHP, and Sect. 14.3 discusses the technical challenges and opportunities for small-scale engines. This chapter reviews ICEs, Stirling engines, Brayton cycle engines, and micro Rankine cycle engines as applicable to micro-CHP applications. It is noted here that fuel cells are one of the most sought-after technologies for CHP as they can deliver higher fuel-to-electrical conversion efficiency (30–60%) at small (1–1.5 kW) scales (Maghanki et al. 2013). However, they are not reviewed in this chapter as their economics are thought to be severely challenged at small scales due to their high capital and maintenance costs (Sevier 2015).

14.2 Review of the State of the Art for Small CHP Systems

The following classes of generators are reviewed in their respective subsections, viz. reciprocating ICEs, Stirling engines, Brayton cycle engines, and micro-Rankine cycle engines.

Reciprocating ICEs are good candidates for micro-CHP applications from fuel conversion efficiency and load-following capability standpoints. However, they require periodic maintenance in terms of oil change, replacement of spark plugs and/or fuel injectors, and occasional replacement of power cylinder components and emissions after-treatment devices. Spark-ignited NG ICEs can be broadly classified as stoichiometric and lean burn ICEs. Stoichiometric ICEs (without exhaust gas dilution) tend to be lower in fuel conversion efficiency as compared to lean burn ICEs (for reasons discussed in Sect. 14.3); however, stoichiometric ICEs tend to have lower tailpipe-out emissions as a low-cost catalytic converter can be used to oxidize carbon monoxide (CO) and hydrocarbons (HC) while simultaneously reducing oxides of nitrogen (NO_x). Lean burn engines are plagued with higher engine-out emissions of CO and HC; however, they lead to lower engine-out NO_x emissions due to lower combustion flame temperatures. Since lean burn engines are characterized by lower exhaust gas temperatures, exhaust after-treatment devices with high conversion efficiencies at traditional catalyst light-off temperatures (~200–250 °C) or even lower temperatures are required.

This is an active and ongoing research area in the ICE community. The limiting factors for high-efficiency ICEs include high heat transfer losses due to the large surface area-to-volume ratios at small scales, incomplete combustion, and friction losses. Stoichiometric ICEs are better suited for load following when compared to lean burn ICEs. Finally, ICEs are well suited to operate with NG with fairly constant composition (e.g. methane number and fuel lower heating value) and will require sophisticated combustion controls to accommodate significant variation in fuel composition. This is critical from a product development perspective as the quality of natural gas varies for each state (and sometimes with season) within the USA.

Stirling engines have the ability to operate for a long period of time without requiring significant maintenance, as evidenced by those employed in space applications, and are characterized by low noise operation. They tend to have lower fuel conversion efficiencies as compared to reciprocating ICEs and are not typically suitable for load following due to their high thermal inertia. However, since it is an external combustion engine, a Stirling engine is robust to changes in fuel composition as it is a heat engine that only requires a temperature differential to operate. In addition, the emissions generated from typical Stirling engine combustors are lower when compared to ICEs. NO_x emission formation is potentially averted due to lower combustion flame temperatures. HC and CO emissions are mitigated due to the higher residence time that is available for their oxidation, when compared to ICEs. Achieving efficient heat transfer between the combustion system and the Stirling engine working fluid is recognized as the chief limiting factor for the development of a high-efficiency Stirling engine. Consequently, the lower fuel-to-electrical conversion efficiency of a Stirling engine will lead to higher heat being rejected from the system (through exhaust gases and coolant), which can be recovered for residential heating. Hence, Stirling engines are better suited for regions with a large thermal load requirement.

Brayton cycle engines are arguably the least mature technology at residential CHP scale. Micro-turbines are the most common Brayton cycle engines employed for micro-CHP applications and are essentially low-powered versions of gas turbines that are used for power generation. Typical power outputs of micro-turbines range from tens to a few hundred kW but are generally considered more mature for applications over 20 kW. To the best of our knowledge, there is only one commercially available micro-turbine product that is less than 5 kW. Some major hurdles that make micro-turbines (employing traditional radial type turbomachinery) inefficient are: (1) small-scale effects leading to high viscous losses in the turbine passages due to low Reynolds number flow, (2) manufacturing tolerances and bearing limitations at high rotational speeds, (3) higher heat transfer due to high surface-to-volume ratios, and (4) high mechanical or parasitic losses. Recuperated Brayton cycle engines, which employ a recuperator for harvesting exhaust gas energy for heating combustion air, are more efficient and expensive as compared to non-recuperated Brayton cycle engines. Thus, Brayton cycle engines at the 1–10 kW scale have low fuel conversion efficiency when compared to ICEs and consequently are better suited for regions with a large thermal load requirement. Like Stirling engines, Brayton cycle engines are also more robust to changes in fuel

composition when compared to ICEs. The emissions generated from Brayton cycle engines are also potentially lower when compared to ICEs for the same reasons stated above for Stirling engines.

Table 14.1 provides a summary of various state-of-the-art generators in each of these categories and their performance metrics including LHV-based

Table 14.1 Summary of the state-of-the-art generators for CHP with capacity less than 10 kW (Honda Worldwide 2018; Barbieri et al. 2012; De Paepe et al. 2006; Aisin 1.5 kW internal combustion engine CHP 2016; CP5WN 2018; CP10WN 2018; Qnergy SmartBoiler 2018; Guyer 2016; EnerTwin 2018) (<https://www.mtrigen.com/>, http://micro-chp.com/micro_chp_products.htm)

	Electric power (kW)	Thermal power (kW)	Fuel energy (kW)	Electric efficiency (%)	Thermal efficiency (%)
<i>ICEs</i>					
Honda Ecowill	1.0	3.3	5.0	20.0	66.0
Honda EXlink MCHP1.0K2	1.0	2.5	3.8	26.3	65.7
Aisin Coremo	1.5	3.7	5.8	26.0	64.0
AISIN SEIKI GECC46A2	4.6	10.6	18.0	25.6	58.6
Marathon Engine Systems' ecopower	4.7	12.5	18.8	25.0	65.0
SenerTec. (Dachs.) HKA G 5.0	5.0	12.1	19.2	26.0	63.1
Yanmar CP5WN	5.0	10.0	17.8	28.0	56.0
Yanmar CP10WN	10.0	16.9	31.5	31.5	53.5
M-TriGen PowerAire 45	3.4	13.0	29.6	11.5	43.9
M-TriGen PowerAire 65	6.0	16.7	37.9	15.8	44.1
M-TriGen PowerAire 85	8.0	21.5	48.9	16.4	44.0
<i>Stirling engines</i>					
Microgen	1.0	6.0	7.4	13.5	81.1
Infinia	1.0	6.4	8.0	12.5	80.0
Baxi Ecogen	1.0	5.0	6.5	15.4	77.0
Navien HYBRIGEN	1.0	5.7	6.5	15.4	88.0
Stirling systems—SOLO161	2.0	8.0	10.0	20.0	80.0
SUNMACHINE	3.0	10.5	14.9	20.1	70.5
Disenco	3.0	12.0	16.3	18.4	73.6
Qnergy SmartBoiler	7.2	39.6	47.1	15.3	84.0
<i>Brayton cycle engines</i>					
MTT EnerTwin	3.2	15.6	20.0	16.0	78.0
<i>Micro-Rankine cycle engines</i>					
Energetix	1.0	8.0	10.0	10.0	80.0
Flow energy's flow boiler	1.0	11.2	13.0	7.7	85.8
OTAG	2.0	16.0	19.1	10.4	83.6
COGEN Microsystems	2.5	11.0	13.5	18.5	81.4

Note that the M-TriGen products are micro-combined cooling, heat, and power (micro-CCHP) systems and their cooling loads are not included here

fuel-to-electrical conversion efficiency and thermal efficiency (ratio of thermal energy to fuel energy) (Honda Worldwide Honda Worldwide|Power products 2018; Barbieri et al. 2012; De Paepe et al. 2006; Aisin 1.5 kW internal combustion engine CHP 2016; CP5WN 2018; CP10WN 2018; Qnergy SmartBoiler 2018; Guyer 2016; MTT EnerTwin 2018) (<https://www.mtrigen.com/>, http://micro-chp.com/micro_chp_products.htm). The total CHP efficiency is the sum of the fuel-to-electrical conversion efficiency and the thermal efficiency.

14.2.1 Internal Combustion Engines

ICEs are ubiquitous in numerous industrial, transportation, and power generation applications through their high fuel to shaft power conversion efficiencies and their relatively low cost. This efficiency advantage versus competing engine technologies is evident in Fig. 14.2, where the ICEs are shown to have the highest electric

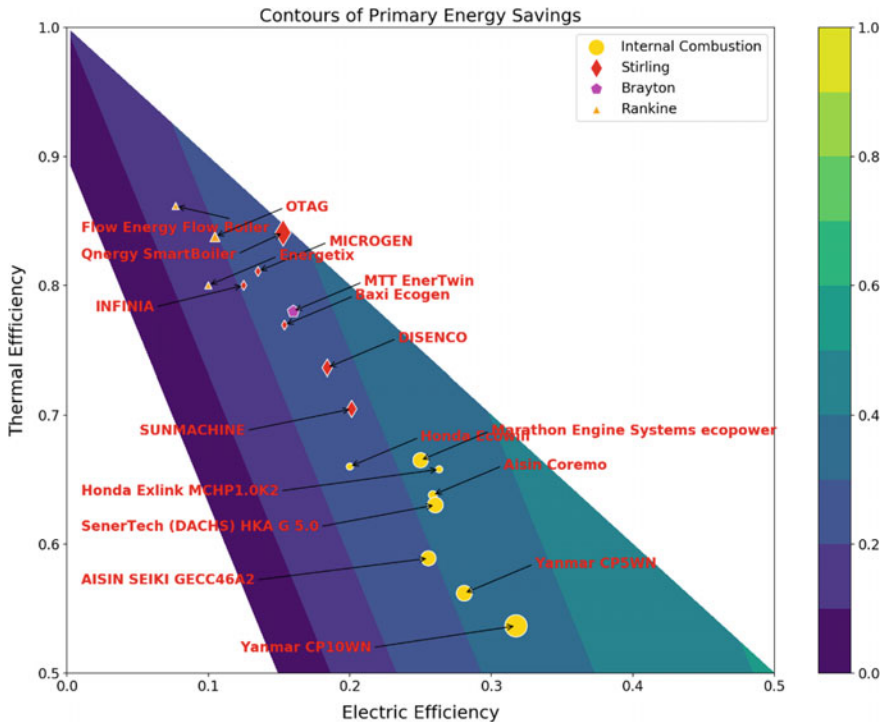


Fig. 14.2 Scatter plot of thermal versus electric efficiency for various CHP systems listed in Table 14.1 overlaid on a contour plot of the maximum potential primary energy savings assuming a baseline electrical grid efficiency of 33.6% (the US average in 2017) and a baseline furnace efficiency of 90% (the marker size is proportional to the maximum electric output of the system)

efficiencies of the cycles represented. Two systems with industry-leading performance at small scales are the Honda EXlink at 1 kW and the Yanmar CP10WN at 10 kW.

The Honda NG or liquid propane-powered Extended Expansion Linkage Engine (EXlink) (Honda Worldwide 2018) employs an over-expanded Atkinson cycle where the expansion stroke volume (163 cm^3) is higher than the compression stroke (110 cm^3), which results in an increased in-cylinder work extraction. In addition, the shorter intake stroke also results in lower pumping losses though at a marginal cost of volumetric efficiency. Thus, the combined effects of increased expansion work and reduced pumping losses result in a higher brake thermal efficiency (defined as the ratio of the brake or shaft power to the fuel energy) for the engine. In addition, the thermal efficiency is as high as 66% by improved cooling system design and integration of the heat exchanger with the catalytic converter (or three-way catalyst). Coupled with these benefits, the system is also quiet in operation with a noise level of 43 dBA. From a reliability standpoint, the maintenance interval is around 6000 h of use or 3 years (whichever is earlier) due to the use of long-life spark plugs and high-capacity oil tank. Recently, Honda has discontinued ICEs from its portfolio of micro-CHP products in Japan as the Japanese market has largely shifted toward fuel cells (Ashurst 2016, 2018).

The Yanmar CHP family of engines (CP5WN 2018; CP10WN 2018) employs an over-expanded Miller cycle along with lean NG combustion (Yanmar mCHP 2016). The fuel-to-electrical conversion efficiencies for the 5 and 10 kW systems are 28% and 31.5%, respectively, with more than 50% thermal efficiencies. Along with high efficiency, lean NG combustion also results in low thermal NO_x emission as it reduces the in-cylinder flame temperatures. The noise levels for the 5 and 10 kW engines are 51 and 54 dBA, respectively, while the reported maintenance interval for both the products is 10,000 h of operation.

Figure 14.3a, reproduced from Cullen and McGovern (2010), illustrates the general trends in the fuel energy balance of industrial ICEs at various engine brake powers at a constant speed of 1500 rpm. Figure 14.3b, reproduced from Muccillo and Gimelli (2014), shows the estimated energy balance for a 15 kW ICE-based CHP generator.

In Fig. 14.3a, the jacket water accounts for both engine friction and engine heat transfer losses. It can be clearly seen that the heat transfer is highly nonlinear and increases significantly (>35% of the total fuel energy) at low rated powers. Moreover, the available exhaust energy has an inverse relationship with respect to heat transfer; i.e. the fraction of exhaust energy decreases with a reduction in engine power, while the converse is true for heat transfer. As the pie-chart in Fig. 14.3b shows, the total irrecoverable losses account for about 14% of the fuel energy (sum of alternator loss, wall heat transfer loss, and exhaust gas loss), thus yielding a total CHP efficiency of 86%. However, only 28% of the fuel energy is converted into electricity while the remaining energy is captured by the engine cooling circuit, exhaust gases, and the radiator heat exchanger.

More recently, Taie et al. (2018) performed detailed analyses on the 1-kW Honda Ecowill CHP system using the first and second law of thermodynamics. This

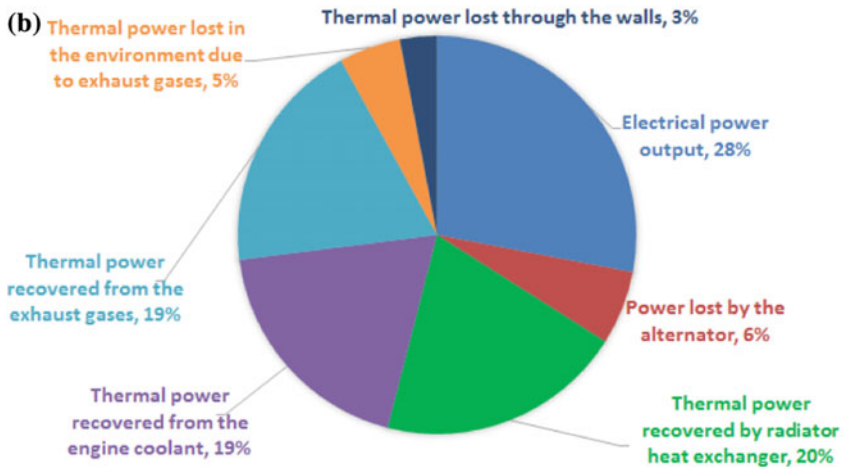
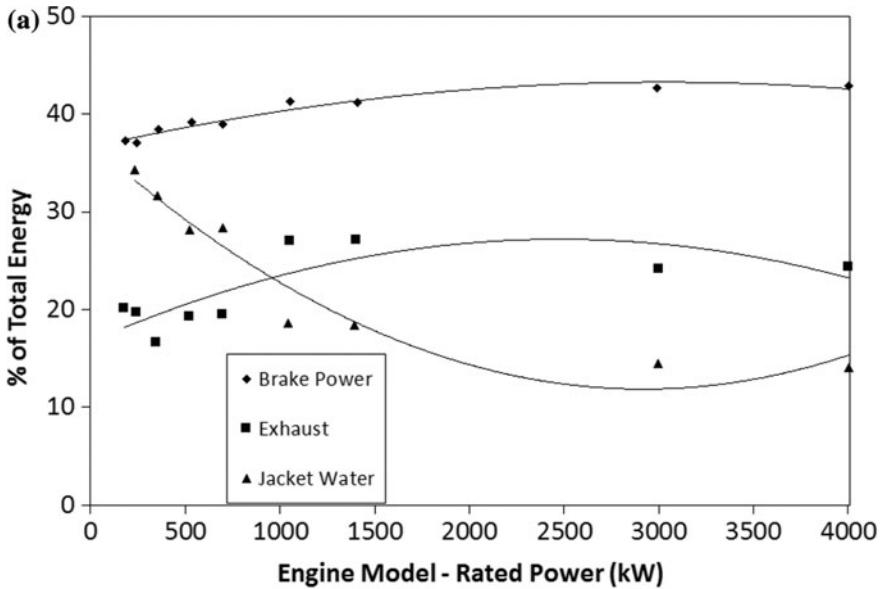


Fig. 14.3 a Energy breakdown of industrial ICES as a function of engine brake power reproduced from Cullen and McGovern (2010) and b 15 kW ICE CHP energy breakdown reproduced from Muccillo and Gimelli (2014)

work was funded by the US Department of Energy (DOE), Advanced Research Projects Agency-Energy (ARPA-E). They performed both a CHP system-level and an ICE-level energy and exergy flow analyses. Figure 14.4a–d [reprinted from Taie et al. (2018)] shows the energy and exergy flows based on the first law and second law analyses, for both the CHP and ICE systems. The three colored bars represent

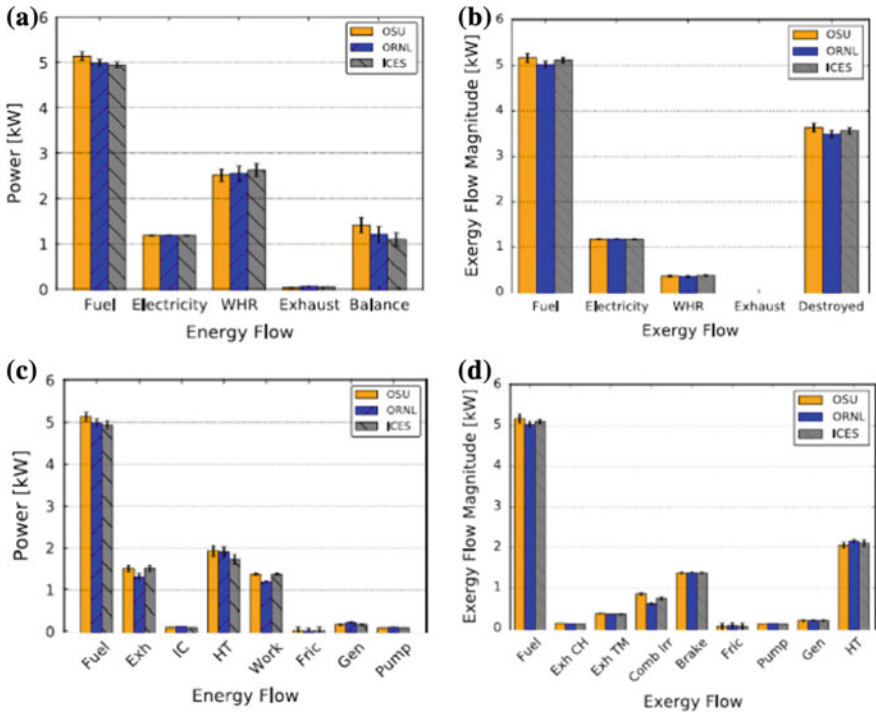


Fig. 14.4 **a** Energy flows calculated by the first law analysis for the CHP system, **b** exergy flows calculated by the second law analysis for the CHP system, **c** energy flows calculated by the first law analysis for the ICE, and **d** exergy flows calculated by the second law analysis for the ICE (Taie et al. 2018)

experimental tests that were conducted at three different facilities, illustrating the experimental repeatability. A 23% fuel-to-electrical conversion efficiency is obtained based on the first law analysis. The first law waste heat recovery (WHR) energy from Fig. 14.4a represents the energy that can be captured for hot water and space heating purposes. The WHR exergy as per Fig. 14.4b represents the maximum fraction of the WHR energy that can be converted into useful work using a bottoming cycle device such as an organic Rankine cycle. Figure 14.4c shows the energy flows for the Honda Ecowill ICE prime mover. The Work term in the figure represents the brake work, and the electrical work can be obtained after the deduction of the generator/alternator losses (Gen) from the brake work. Part of the exhaust (Exh) and heat transfer (HT) is captured as waste heat for heating. Additional loss mechanisms include powertrain friction (Fric), incomplete combustion (IC), and pumping losses (Pump). Finally, Fig. 14.4d shows the exergy flows for the ICE. The exhaust exergy is split into exhaust thermomechanical exergy (Exh TM) and exhaust chemical exergy (Exh CH). Notably, the exergy loss

due to combustion (Comb Irr) is a major loss mechanism predominantly due to flame propagation in stoichiometric combustion.

Significant challenges exist to obtain high brake thermal efficiencies (and hence high fuel-to-electrical conversion efficiency) from small-size and low-power ICES due to high surface-to-volume ratios that lead to high heat transfer. This can be shown by a simple back-of-the-envelope calculation. Consider four different ICE bore sizes ($b = 0.1, 0.08, 0.05,$ and 0.025 m), a bore-to-stroke ratio of 0.8, an engine speed of 1500 rpm, a thermal conductivity (K) of the in-cylinder fluid of 0.06 W/m/K, and a dynamic viscosity of the in-cylinder fluid (ν) of 0.0001 m²/s; the mean piston speed (S_p) can be calculated using the engine speed and stroke length. The Nusselt number (Nu) and the convective heat transfer coefficient (h) can be calculated using the Taylor correlation (Taylor 1985) as shown in Eq. (14.1).

$$\text{Nu} = \frac{h \cdot b}{K} = 10.4 \cdot \left(\frac{S_p \cdot b}{\nu} \right)^{0.75} \quad (14.1)$$

An average in-cylinder gas temperature of 1500 K and an oil temperature of 353 K were assumed for all the cases. The cycle-averaged heat transfer was calculated using Eq. (14.2).

$$Q = h \cdot A \cdot \Delta T \quad (14.2)$$

where A is the reference area calculated using the cylinder bore and ΔT is the heat transfer potential, which is the difference between the average in-cylinder gas temperature and oil temperature. The brake power can be calculated using the engine displacement and by assuming a constant power density of 65 kW/L for all the cases. Figure 14.5 shows the ratio of the engine heat transfer to brake power as a function of engine brake power. Though the model is rudimentary, it alludes to meaningful insights into the relative contribution of fuel energy to engine heat transfer and useful brake power. It is also interesting to note that the energy associated with engine heat transfer is higher than the useful brake power for small kW engines (<5 kW), a trend that is also shown in the experimental data in Fig. 14.4c where HT is greater than the Work term. Additionally, at the small engine scales, incomplete combustion is a significant contributor to inefficiency predominantly due to flame-wall interaction (heat transfer between flame and cold wall and subsequent flame quenching) and crevice flows.

In terms of costs, the Ecowill and EXlink systems are estimated to be about \$13,000 and \$24,000, respectively, while the ecopower 4.7 kW is estimated to cost about \$24,000. These costs are based on customer input of those systems and just serve as a ballpark indicator rather than precise values. Part of the reason for the high cost of these systems is their low-volume production, which is expected to be alleviated with increased penetration of residential CHP.

Thus, novel strategies for reducing in-cylinder heat transfer, incomplete combustion, pumping, friction, and innovative combustion strategies are needed to deliver higher fuel-to-electrical conversion efficiency for small-scale ICES. In

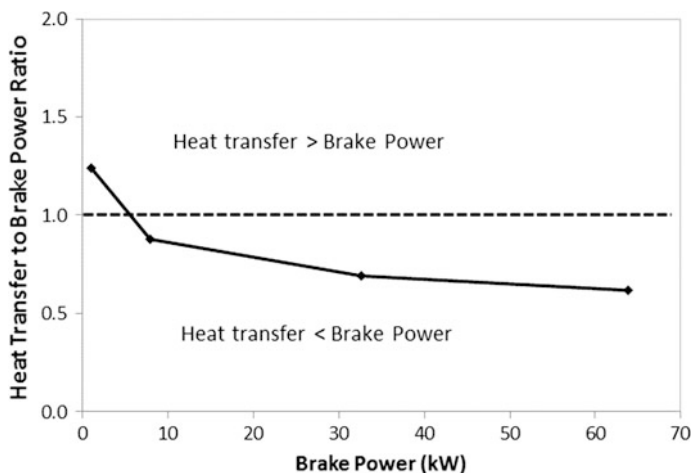


Fig. 14.5 Ratio of engine heat transfer to brake power as a function of engine brake power

addition, a significant emphasis on the reduction of the total installed cost is necessary to make these technologies feasible for residential customers. As noted by Ashurst (2016), the ICE system cost is about 60% of the total installed cost to the customer.

14.2.2 Stirling Engines

Stirling engines are arguably the most mature external combustion engines that have penetrated the CHP market. Table 14.1 shows the efficiency of several commercially available Stirling engines for less than 10-kW micro-CHP applications. As seen from the table, all the Stirling engines have less than 20% fuel-to-electrical conversion efficiency at 1 kW. It is important to note that the total CHP efficiency can exceed 90% for such systems. The total CHP efficiency of the Navien HYBRIGEN system is claimed to be more than 100% on a LHV basis (note the efficiency is less than 100% on a fuel higher heating value basis) due to the use of a condensing boiler for heat capture.

Figure 14.6a, reprinted from Valenti et al. (2014), shows a Sankey diagram for a Stirling engine generator with typical system losses. A significant portion of fuel energy is lost in the exhaust gases and some to the burner cooling water, while the remaining portion of the fuel energy is used as heat input to the Stirling engine. The ratio of the useful heat input to the fuel energy represents the combustor efficiency (η_{comb}). Furthermore, the fraction of the useful heat input, which is converted into mechanical work by the Stirling engine working fluid (after taking into account the engine heat transfer loss) represents the Stirling engine indicated closed-cycle work. The ratio of the indicated closed-cycle work to the Stirling engine useful heat input

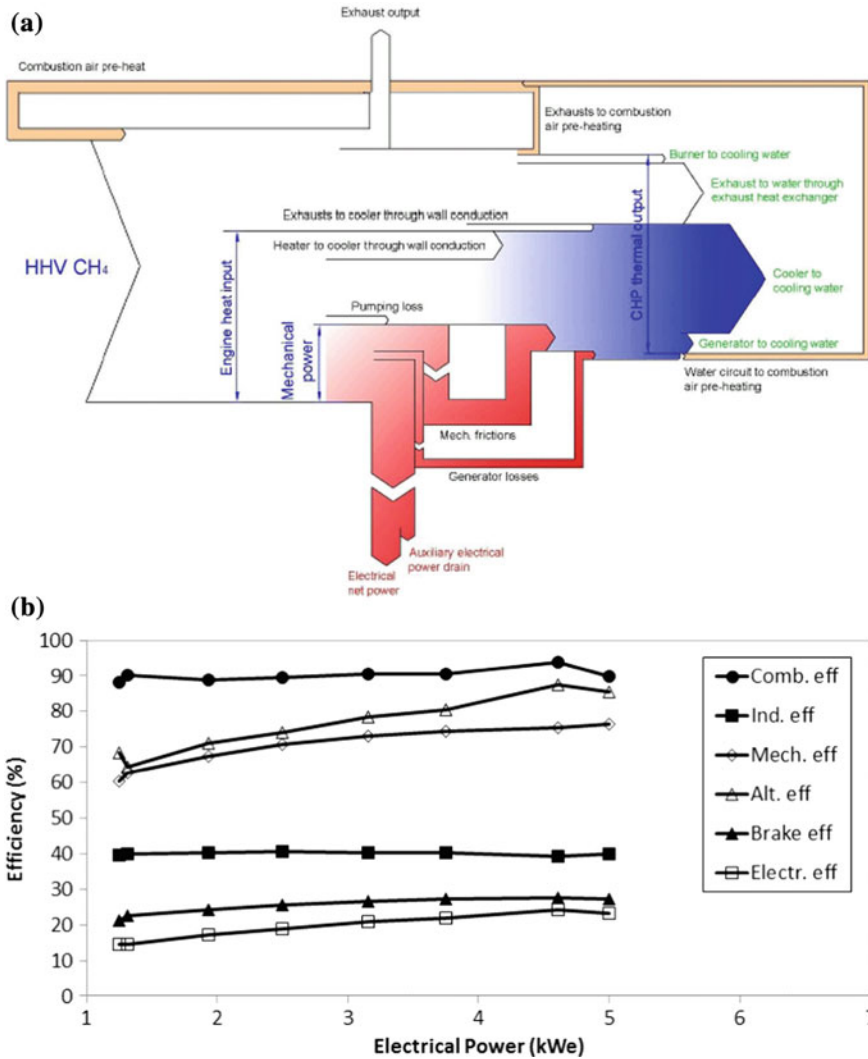


Fig. 14.6 **a** Sankey diagram for a Stirling engine-driven CHP system from Valenti et al. (2014) and **b** typical state-of-the-art small-scale Stirling engine efficiency breakdown reproduced from García et al. (2014)

represents the indicated cycle efficiency (η_{ind}). Some portion of the indicated work is further lost in pumping, friction, and other parasitic losses yielding the net shaft work. The ratio of the shaft work to the indicated work gives the mechanical efficiency (η_{mech}). Finally, the alternator efficiency (η_{alt}), which is the ratio of electrical power to the shaft power, represents the portion of shaft work that is converted into useful electrical power. In a typical CHP system as shown in

Fig. 14.6a, much of the energy lost in the exhaust and coolant (heat transfer and friction) is recovered for residential hot water and space heating purposes. Using a recuperator, the exhaust heat can also be used for preheating combustion air for improving the combustor efficiency. Thus, for an external combustion engine, the energy cascade gives an expression for the fuel-to-electrical conversion efficiency (η_e) as shown in Eq. (14.3):

$$\eta_e = \eta_{\text{comb}} \cdot \eta_{\text{ind}} \cdot \eta_{\text{mech}} \cdot \eta_{\text{alt}} \quad (14.3)$$

Figure 14.6b, reproduced from García et al. (2014), shows the efficiency breakdown for a kinematic Stirling engine running at 1500 rpm operating with NG as fuel and helium as the working fluid with a maximum working gas temperature of 625 °C. The subsystem efficiency data were obtained by García et al. (2014) using a combination of experimental measurements (e.g. thermal and electrical power outputs) and empirical models that were developed using experimental data from different prototype Stirling engines. In their experiments, the load was varied as a function of the working gas pressure. In Fig. 14.6b, brake efficiency (or brake thermal efficiency, η_{br}) can be defined as shown in Eq. (14.4):

$$\eta_{\text{br}} = \eta_{\text{comb}} \cdot \eta_{\text{ind}} \cdot \eta_{\text{mech}} \quad (14.4)$$

The indicated cycle efficiency is around 40% irrespective of the load and is primarily a function of the working gas temperature (625 °C in this case). Higher working gas temperatures can enable better indicated efficiencies due to higher Carnot cycle efficiency. In addition, the mechanical efficiency plummets at the lower power levels, which indicates that lowering engine friction (e.g. employing a free-piston Stirling engine) and parasitic losses is crucial for obtaining higher engine efficiencies. In addition, reducing the parasitic losses in power converters and power electronics will also be a key enabler for improving fuel conversion efficiency. These are accounted for in the alternator efficiency. Finally, the combustor efficiency can also be improved by improving burner design, such as employing a recuperated burner for preheating air, and by lowering the convective heat losses from the burner system. A detailed discussion of the challenges in integrating an efficient combustion system with the Stirling engine is provided in Sect. 14.3.2.

One of the reasons why Stirling engines are considered better for micro-CHP applications is that they can run continuously at steady-state conditions without needing any maintenance over a long period of time. The estimated cost of 1-kW Stirling engine CHP systems is expected to be of the same order of magnitude as an equivalent ICE and thus faces a similar challenge in achieving high market penetration. For example, a study by Ferreira et al. (2016) estimates a total capital cost of 25,880 € for a solar-powered Stirling engine with an electrical power output of 3.65 kW for residential micro-CHP. As noted by Ashurst (2016), the Stirling engine system cost is only about 30% of the total installed cost to the customer.

14.2.3 Brayton Cycle and Micro Rankine Cycle Engines

Recuperated micro-turbines are the most common Brayton cycle engines employed for micro-CHP applications. As noted before, major technical hurdles for micro-turbines include high viscous losses in the turbine passages due to low Reynolds number flow, manufacturing tolerances, bearing limitations at high rotational speeds, high heat transfer, and high mechanical or parasitic losses. In addition, the cost associated in manufacturing a small-scale turbine with precision tolerances is also high.

One of the smallest micro-turbine systems, a prototype 3-kW system (15 kW thermal load) for CHP applications, was built by Micro Turbine Technology BV (MTT) and is being commercialized under the name EnerTwin (2018). One of the earlier prototype systems demonstrated 16% fuel-to-electrical conversion efficiency and 80% thermal efficiency (Visser et al. 2012). Figure 14.7, reproduced from Visser et al. (2011), shows energy losses for the 3 kW micro-turbine from an experimental rig test. The numbers reported in the schematic are a percentage of fuel energy. Much of the fuel energy is lost in the exhaust (47.0%) and the rest as heat losses, friction and parasitic loads (40.8%). The international standard atmosphere (ISA) corrected values for brake and electrical powers obtained in this study were 2.98 and 2.7 kW, respectively, yielding a high value of 91% for the alternator efficiency and 13.5% for the shaft efficiency. The study reports a fuel-to-electrical conversion efficiency of only 12.3% for a recuperated cycle gas turbine system. It is believed that further subsystem improvements and optimization have resulted in an improvement in fuel conversion efficiency (Visser et al. 2012). Since there is a

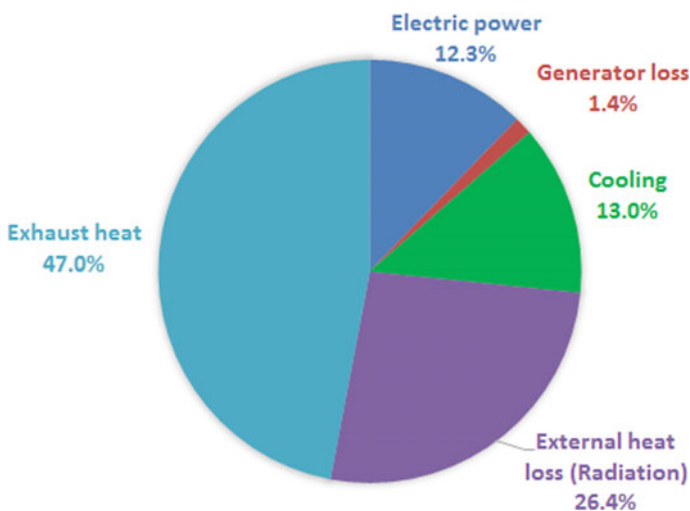


Fig. 14.7 Typical energy losses (% of fuel energy) in a small-scale micro-turbine employing radial turbomachinery. Figure reproduced from Visser et al. (2011)

dearth of commercial technologies at this scale, the system life and product costs are uncertain at this point.

Micro-Rankine cycles are also employed for CHP applications but with much lower fuel-to-electrical conversion efficiencies of around 10–19% for 1–2.5 kW, as shown in Table 14.1. Again, the total CHP efficiency of such systems can exceed 90%. These applications are currently more suitable for replacing the household boiler. In addition, organic Rankine cycles (ORCs) are predominantly used as bottoming cycles for capturing the waste energy typically from an ICE.

14.3 Technical Opportunities and Challenges

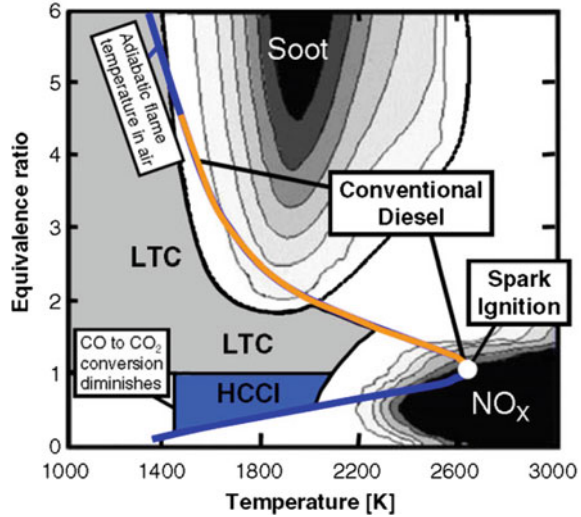
This section provides the technical opportunities and challenges for ICEs, Stirling engines, and Brayton cycle engines. The US Department of Energy, ARPA-E, initiated the GENerators for Small Electrical and Thermal Systems (GENSETS) program in 2015 (GENSETS 2018). The program is funding various mechanical and heat engine technologies with the goal of achieving 40% fuel-to-electrical conversion efficiency at 1-kW electrical output and is targeted primarily at residential CHP. Technical project highlights from the GENSETS program are included in the relevant sections.

14.3.1 Internal Combustion Engines

For several decades, the ICE community has been developing low-temperature combustion (LTC) strategies such as homogenous charge compression ignition (HCCI), premixed charge compression ignition (PCCI), and high exhaust gas recirculation (EGR) LTC to achieve both high efficiency and mitigate NO_x and particulate matter (PM) emissions. Most of the LTC strategies however struggle with higher hydrocarbon (HC) and carbon monoxide (CO) emissions. Figure 14.8, reprinted from Dec (2009), shows the classic equivalence ratio (Φ)–temperature (T) plot overlaid with different combustion regimes. HCCI combustion has a fairly narrow operating range, and below an operating temperature of 1400 K, the conversion of CO to CO_2 (through the reaction $\text{CO} + \text{OH} \rightarrow \text{CO}_2 + \text{H}$) diminishes. It is also characterized by low soot and NO_x production, which makes it attractive for transportation and power generation applications. Since the operation regime is narrow and since HCCI combustion is characterized with high pressure rise rates (due to high charge homogeneity), transient and high load operation of HCCI engines are both challenging, and hence, HCCI is best suited for single-point or steady-state operation such as those seen in power generation engines and CHP applications.

Kobayashi et al. (2011) demonstrated 43.3% brake thermal efficiency and estimated a 40% fuel-to-electrical conversion efficiency for a 50-kW boosted NG

Fig. 14.8 Φ - T plot showing HCCI and LTC combustion regimes with soot and NO_x islands (Dec 2009)

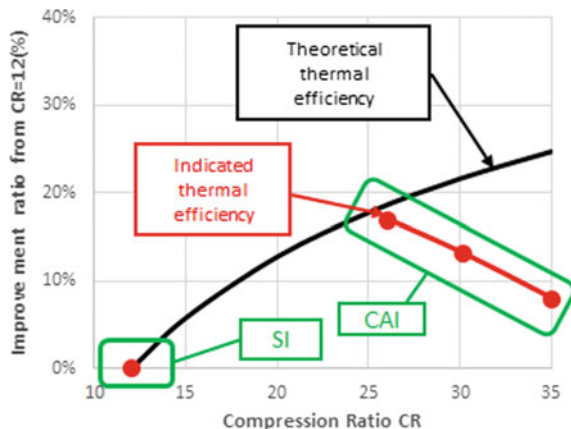


engine. The engine-out NO_x emission reported in their study, without employing an exhaust after-treatment device, was about 14 ppm. Optimizations of the compression ratio (CR) and boost pressure were performed to obtain high combustion efficiencies and low emissions of NO_x and CO. However, under high-efficiency operating conditions, the engine was also found to be sensitive to knocking. Dilution concepts such as high EGR LTC technologies predominantly reduce the heat transfer from the working fluid by operating at lower local temperatures (hence lower temperature gradients) and also by increasing the in-cylinder ratio of the specific heats (γ) thus attaining higher fuel conversion efficiencies.

Caton (2014) published a study that shows potential pathways for attaining indicated efficiencies of over 50% and brake thermal efficiencies of over 45% by using a simple spark-ignited Otto cycle thermodynamic simulation for automotive engines. Key drivers for efficiency gain included increasing CR, reducing burn duration, lean engine operation (excess air ratio (λ) ~ 1.4), and high EGR ($\sim 45\%$). The model predicted a significant reduction in engine heat loss from 15.6% (baseline) to 5% of fuel energy. This improvement is predominantly attributed to lean combustion and high EGR operation. The main contributions to high engine efficiency were attributed to the increased ratio of specific heats and reduced in-cylinder heat transfer.

Killingsworth et al. (2011) operated a hydrogen–oxygen–argon engine and compared its performance with a hydrogen–air engine. The exhaust of the argon engine, which is composed of water vapor and argon, was condensed to recirculate the argon back into the engine intake as diluent. Since the γ of argon is 1.6, the hydrogen–oxygen–argon engine was more efficient than the hydrogen–air engine by about 10% points at a CR of 6. The hydrogen–oxygen–argon engine, however, could not be operated at higher CR as it was susceptible to engine knock caused by

Fig. 14.9 Comparison of theoretical Otto cycle efficiency versus actual efficiency as a function of CR reproduced from Koga and Kiura (2013). The red line shows the effect of increasing surface area-to-volume ratio



higher local temperatures, which is again attributed to the high γ of the mixture. One of the issues with this approach is its limited application with hydrocarbon fuels, such as NG, as the separation of argon from the exhaust gases is challenging.

Another intriguing study by Koga and Kiura (2013) from Honda R&D Co. looked at the co-optimization of CR and stroke-to-bore ratio for increasing the efficiency for a small NG engine. This approach aimed at reducing heat transfer in, what they term as, the controlled autoignition (CAI) combustion mode (pseudonym for HCCI). It was observed that the engine efficiency improved by purely increasing the CR until a certain point (CR = 25 in their study) and then plummeted due to the subsequent high surface area-to-volume ratios (and hence high heat transfer losses), when the piston was at the top dead center. This is in sharp contrast to the monotonic increase in thermal efficiency (η_{th}) that is expected from the classic Otto cycle relationship ($\eta_{th} = 1 - 1/CR^{\gamma-1}$). This is illustrated in Fig. 14.9, which is reproduced from Koga and Kiura (2013).

In order to reduce the heat transfer, a simultaneous stroke-to-bore ratio optimization was also performed at a CR of 26, which reduced the surface area-to-volume ratio from 9.1 to 5.8 for a corresponding change in the stroke-to-bore ratio from 1 to 2.1. With a stroke-to-bore ratio of 2.1 and a CR of 26, the engine yielded a net brake thermal efficiency of 39.1%, which was 9.2% points higher than the baseline engine efficiency.

Gangopadhyay et al. (2012) investigated strategies to reduce engine friction using surface finishing and coating materials such as manganese-phosphate and diamond-like coating (DLC). In their study, a maximum of 17–25% friction improvement was seen at various speeds of engine operations. Further improvements could also be made with advanced lubrication technologies. To improve the efficiency of modern ICEs, Cheng et al. (2014) investigated individual lubricant formulations applicable to different engine subsystems yielding an optimum combination of lubricant formulations for the overall system. In their study, a mechanical efficiency improvement of over 5% was observed when operating a

16 hp Kohler twin cylinder diesel engine with different multi-grade oil formulations in the valvetrain and power cylinder subsystems. Furthermore, a friction improvement of over 10% was seen by altering the shear thinning characteristics of the lubricant in a motored valve train.

In terms of in-cylinder heat transfer reduction, there are numerous studies in the literature that employ thermal barrier coatings (TBCs), in an effort to mimic an adiabatic engine, with improved thermal efficiency. Parlak et al. (2005) investigated the effects of TBCs on the piston, cylinder head, and valves of a six-cylinder production diesel engine and only obtained a maximum of 2% improvement in brake thermal efficiency. However, the exhaust energy availability increased by about 3–27% depending on the operating speed and load. It was also noted that a maximum of 47% of the total exhaust energy could be extracted from an exergy standpoint. TBCs have been a long-standing topic of focus in the gas turbine industry; however, ICEs have not been able to completely leverage their advantage due to durability issues that arise from thermal cycling. The use of a bottoming cycle with a thermal barrier-coated ICE is a logical combination to yield high system efficiency.

Other recent technologies to improve brake thermal efficiency for small-scale ICEs include Miller cycle using variable valve timing (VVT) (Fontana and Galloni 2009), Atkinson cycle 10-kW ICE (Capaldi 2014), and free-piston engine linear generator (FPEG) (Kosaka et al. 2014; Goto et al. 2014). One-dimensional cycle simulation of the 10-kW Toyota FPEG (Kosaka et al. 2014; Goto et al. 2014) predicts a thermal efficiency of about 42% using a PCCI strategy.

In the ARPA-E GENSETS program, Wisconsin Engine Research Consultants, LLC (WERC), located in Madison, Wisconsin, USA, in collaboration with University of Wisconsin-Madison, Briggs and Stratton Corporation, and Adiabatics, Inc. is developing a 1-kW spark-assisted HCCI (SA-HCCI) engine (Reitz et al. 2018). The engine has a compression ratio of 17 and a stroke-to-bore ratio of 1.47 and is operated at stoichiometry with EGR dilution. SA-HCCI or spark-assisted compression ignition (SACI) uses a spark plug to initiate combustion, which subsequently leads to end-gas autoignition. In traditional HCCI, ignition is purely governed by chemical kinetics, and hence, achieving the optimum ignition timing at a particular speed and load is challenging. This is because the autoignition of the fuel-air mixture is very sensitive to initial, boundary, and in-cylinder conditions of temperature, pressure, and charge composition. In order to alleviate this problem, a spark plug is used in SACI, which provides the necessary control lever for initiating ignition. As of early 2018, the WERC team's engine has demonstrated a brake thermal efficiency of 34%. Figure 14.10 shows the pathway to 39% brake thermal efficiency and includes various updates, viz. improving cylinder head design, reducing incomplete combustion, reducing friction mean effective power (FMEP), and employing TBC. A three-way catalyst will be used for mitigating emissions of NO_x , CO, and HC. It is noted here that the next-generation Mazda SKYACTIV-X automotive engine will employ spark-controlled compression ignition (SPCCI), which is a variant of SACI (MAZDA: Next-generation technology 2018).

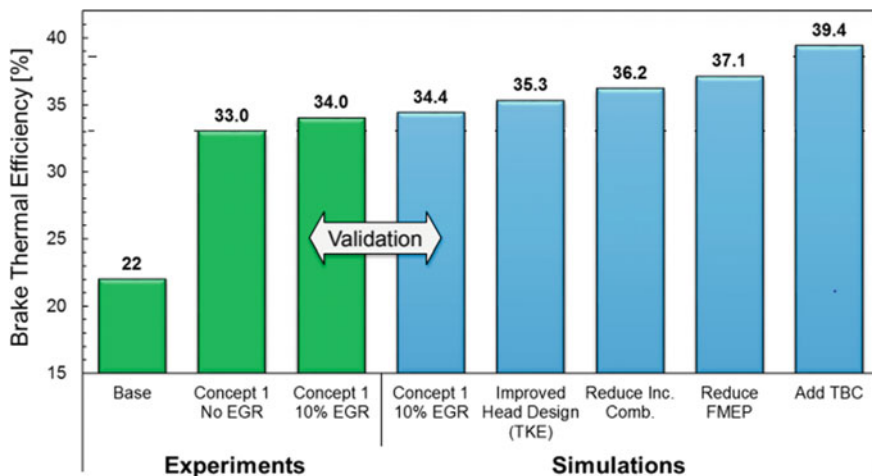


Fig. 14.10 Technical pathway as proposed by WERC to achieve 39% brake thermal efficiency in a 1-kW ICE (Reitz et al. 2018)

Another project lead by Mahle Powertrain, LLC (Plymouth, Michigan, USA) in collaboration with Oak Ridge National Laboratory, IntelliChoice Energy, Kohler Engines, Louthan Engineering, and ExxonMobil has demonstrated, as of early 2018, a brake thermal efficiency of 32.5% at 1.7-kW brake power using their proprietary Mahle jet ignition (MJ) technology (Bunce 2018). MJ is a variant of turbulent jet ignition (TJI) technology and employs a prechamber, which is instrumented with a prechamber injector. A small quantity of fuel is injected in the prechamber where the combustion is initiated typically under rich conditions using a conventional spark plug. The resulting turbulent jets from the partially burned fuel-air mixture in the prechamber emanate into the main chamber through the prechamber nozzle. These jets act as local ignition sources for the main chamber fuel. NG is injected in the main chamber with the help of a port injector where the fuel-air mixture is kept lean. MJ is an enabling technology to extend the ICE lean limit operation, thus significantly improving the thermodynamic and brake thermal efficiencies. Other complementing technologies in this project include low-friction engine components and engine downspeeding for reducing the FMEP. For NO_x , CO, and methane emissions mitigation, the team will be employing a lean NO_x trap and a methane oxidation catalyst that is capable of operating at low exhaust gas temperatures. Figure 14.11a shows a CAD image of the MJ prechamber on the engine cylinder head, and Fig. 14.11b shows the first law energy breakdown that was achieved at a brake power of 1.7 kW and an excess air ratio (λ) of 1.7.

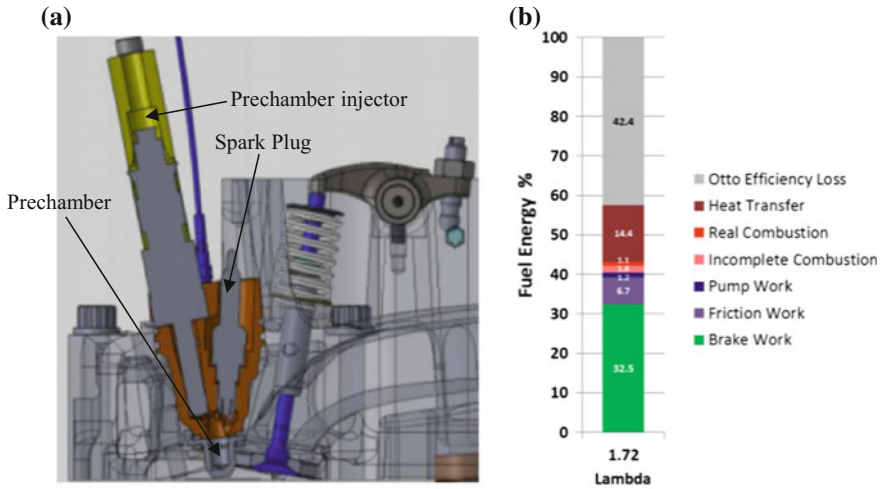


Fig. 14.11 a CAD image of Mahle jet injection (MJ) technology and b first law energy breakdown for the MJ engine at a brake power of 1.7 kW and an excess air ratio of 1.7 (Bunce 2018)

14.3.2 Stirling Engines

One of the critical challenges in Stirling engines (and in other external combustion engines) is to achieve better heat transfer from the combusted fuel to the engine working fluid. The combustor efficiency (η_{comb}) is a measure of effectiveness with which heat is transferred from the fuel to the Stirling engine working fluid. In order to evaluate the combustor efficiency, a simple steady-state modeling analysis was undertaken here. Consider a simple dome-shaped Stirling engine heater head design as shown in Fig. 14.12. Consider a simple NG burner mounted closely to the Stirling heater head, which is transferring heat to the Stirling engine heater head through radiation (Q_{rad}) and convection (Q_{conv}). Radiative heat transfer is assumed to occur between the flame and the heater head dome, while convective heat transfer is assumed to occur between the exhaust gases and the heater head along the length of the heater head. After exchanging heat with the Stirling engine, the exhaust gas is assumed to flow through a recuperator to heat the intake air for the burner (not shown in the figure). The working fluid (generally helium) is enclosed in the heater head, which performs expansion work on a power piston, which in turn drives a linear alternator to produce electricity (not shown in the figure). The details of the engine, combustion system, and the assumptions in the analysis are listed in Table 14.2. Note that the heater head dome temperature is intentionally kept at a lower temperature than the walls for preserving mechanical safety.

A steady-state energy balance analysis was performed on this recuperated burner-engine system using the parameters provided in Table 14.2. The fuel energy

Fig. 14.12 Schematic of a simple burner and dome-shaped Stirling engine heater head configuration

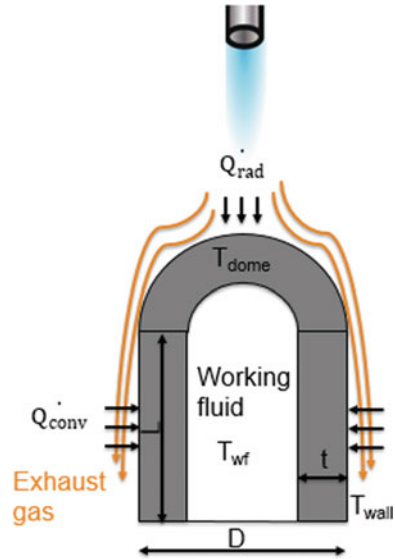


Table 14.2 Assumptions and parameter values for Stirling engine heat transfer analysis

Parameter	Value
Burner diameter—inches	1
Diameter (D) of heater head—mm	80–120
Length (L) of heater head—mm	100–150
Thickness of heater head shell (t)—mm	4
Heater head wall temperature (T_{wall})—°C	600–800
Heater head dome temperature (T_{dome})—°C	$T_{wall} - 25$ °C
Recuperated air temperature—°C	500–615
Fuel (methane) temperature—°C	25
Excess air ratio (λ)	2.5
Turbulence intensity (Tu)	0.05 or 5%
Flame diameter (D_{flame})—mm	$D + 10$ (assuming a hemispherical flame)
Heater head material and thermal conductivity (K_{HH})—W/mK	IN718 and 23.2 at 750 °C
View factor (F_{12}), where 1 denotes dome and 2 denotes flame	1 (Incropera and DeWitt 2002)
Emissivity of heater head material (ϵ_1)	0.33 (Keller et al. 2015)
Emissivity of non-luminous flame (ϵ_2)	0.20 (Sherman 1934)
Recuperator effectiveness	0.9
Heat to mechanical work efficiency of Stirling engine	65% of Carnot efficiency (η_C) operating between working fluid temperature (T_{wf}) and a cold side temperature of 60 °C
Mechanical work to electrical work efficiency or power converter efficiency (η_{pc})	0.9

that is burned is used to transfer heat to the Stirling engine via convection and radiation, and the remaining energy is carried away by the exhaust gases, which is recuperated for heating the intake air from an initial temperature of 25 °C with an effectiveness of 90%. An excess air ratio of 2.5 was chosen to achieve a peak adiabatic flame temperature (T_{flame}) below 1500 °C to mitigate NO_x emissions and to alleviate thermal stresses on the heater head material. For simplicity, the fuel was assumed to be methane (surrogate for NG), the burned gas temperature was assumed to be the same as the adiabatic flame temperature, and the exhaust gas was assumed to have the properties of nitrogen. Temperature-dependent specific heat properties were used in the analysis for the exhaust gases.

Radiation heat transfer was assumed between the flame and the heater head dome. Both the flame and dome were assumed to be concentric hemispheres, and radiation heat transfer (Watts) was calculated using Eq. (14.5) (Incropera and DeWitt 2002). In Eq. (14.5), A_{dome} is the surface area of the heater head dome hemisphere and σ is the Stefan–Boltzmann constant.

$$\dot{Q}_{\text{rad}} = \frac{\sigma \cdot A_{\text{dome}} \cdot (T_{\text{flame}}^4 - T_{\text{dome}}^4)}{\left[\frac{1}{\varepsilon_1} + \left(\frac{1-\varepsilon_2}{\varepsilon_2} \right) \cdot \left(\frac{D}{D_{\text{flame}}} \right)^2 \right]} \quad (14.5)$$

Convection heat transfer was assumed between the exhaust gases and cylindrical portion of the heater head. The turbulent Nusselt number (Nu) correlation, as shown in Eq. (14.6), was used in this case, which is applicable to a flame impinging in a direction normal to a hemi-nosed cylinder in parallel flow (Baukal and Gebhart 1996). The Reynolds number (Re) was calculated using the exhaust gas velocity, dome diameter (characteristic diameter for the flow), and burned gas properties that were evaluated at the burned gas temperature. The exhaust gas velocity was calculated using the exhaust mass flow rate (which is the sum of fuel and air mass flow rates), density of the burned gas, and the burner diameter.

$$\text{Nu} = \text{Re}^{0.5} \left[0.993 + 5.465 \left(\frac{\text{Tu} \cdot \text{Re}^{0.5}}{100} \right) - 2.375 \left(\frac{\text{Tu} \cdot \text{Re}^{0.5}}{100} \right)^2 \right] = \frac{h \cdot D}{K_{\text{gas}}} \quad (14.6)$$

The convection heat transfer coefficient (h) was obtained by calculating the Nusselt number, heater head diameter (D), and thermal conductivity of the burned gas (K_{gas}), which was evaluated at the burned gas temperature. The convective heat transfer to the heater head surface was then calculated using Eq. (14.7) where A_{cyl} is the area of the cylinder and T_b is the burned gas temperature.

$$\dot{Q}_{\text{conv}} = h \cdot A_{\text{cyl}} \cdot (T_b - T_{\text{wall}}) \quad (14.7)$$

At steady-state conditions, the conductive heat transfer rate through the heater head surface was assumed to be equal to the sum of radiative and convective heat transfer rates as shown in Eq. (14.8). For simplicity, the working fluid was assumed

to be at the heater head inner wall temperature. Thus, by knowing the working fluid temperature from Eq. (14.8), the Carnot efficiency of the engine can be obtained. The Stirling engine heat to mechanical work efficiency (η_{ind}) is then obtained from Eq. (14.9), which is assumed to be 65% of the Carnot efficiency (state-of-the-art Stirling engines are typically capable of achieving $\sim 50\%$ of Carnot efficiency). The expression for the combustor efficiency (η_{comb}) is shown in Eq. (14.10), which is obtained from the ratio of the heat transferred to the Stirling engine working fluid to the fuel energy. The fuel energy is calculated using the methane flow rate (m_{fuel}) and methane LHV. The product of the combustor efficiency (η_{comb}), engine heat to mechanical work efficiency (η_{ind}), and the power converter efficiency (η_{pc}) gives the Stirling engine fuel-to-electrical conversion efficiency as shown in Eq. (14.11).

$$\dot{Q}_{\text{rad}} + \dot{Q}_{\text{conv}} = -K_{\text{hh}} \cdot (A_{\text{cyl}} + A_{\text{dome}}) \cdot (T_{\text{wall}} - T_{\text{wf}}) \quad (14.8)$$

$$\eta_{\text{ind}} = 0.65 \cdot \left(1 - \frac{60 + 273.15}{T_{\text{wf}} + 273.15} \right) \quad (14.9)$$

$$\eta_{\text{comb}} = \frac{\dot{Q}_{\text{rad}} + \dot{Q}_{\text{conv}}}{m_{\text{fuel}} \cdot \text{LHV}} \quad (14.10)$$

$$\eta_{\text{e}} = \eta_{\text{comb}} \cdot \eta_{\text{ind}} \cdot \eta_{\text{pc}} \quad (14.11)$$

Figures 14.13, 14.14, 14.15, and 14.16 show the sensitivity of the combustor efficiency and fuel-to-electrical conversion efficiency for the Stirling engine with respect to the air temperature at recuperator outlet location (Fig. 14.13), heater head area by varying the heater head dome diameter (Fig. 14.14), heater head area by varying the heater head length (Fig. 14.15), and heater head surface temperature (T_{wall}) (Fig. 14.16). The black lines with closed square symbols in the figures show the efficiencies when both convection and radiation heat transfer are taken into account, while the black lines with closed circle symbols show the efficiencies with only convection heat transfer (i.e. neglecting radiative heat transfer).

As shown in Fig. 14.13, a higher degree of recuperation is a critical requirement to achieve a high combustor efficiency and hence a high fuel-to-electrical conversion efficiency. Increasing the area by increasing the length of the heater head (Fig. 14.15) leads to better heat transfer than that achieved by increasing the diameter of the heater head (Fig. 14.14). As expected, the effect of radiation is more pronounced by varying the diameter than by varying the heater head length. The increase in heater head temperature and its effect on the efficiencies show an interesting and perhaps counterintuitive trend (Fig. 14.16). Under the assumptions in Table 14.2, an increase in heater head temperature up to 700 °C is effective for improving the fuel-to-electrical conversion efficiency. Any further increase in heater head temperature results in a decrease in fuel-to-electrical conversion efficiency, as shown in Fig. 14.16b. This is because the combustor to Stirling engine heat transfer rate reduces with an increase in the heater head temperature, as shown in

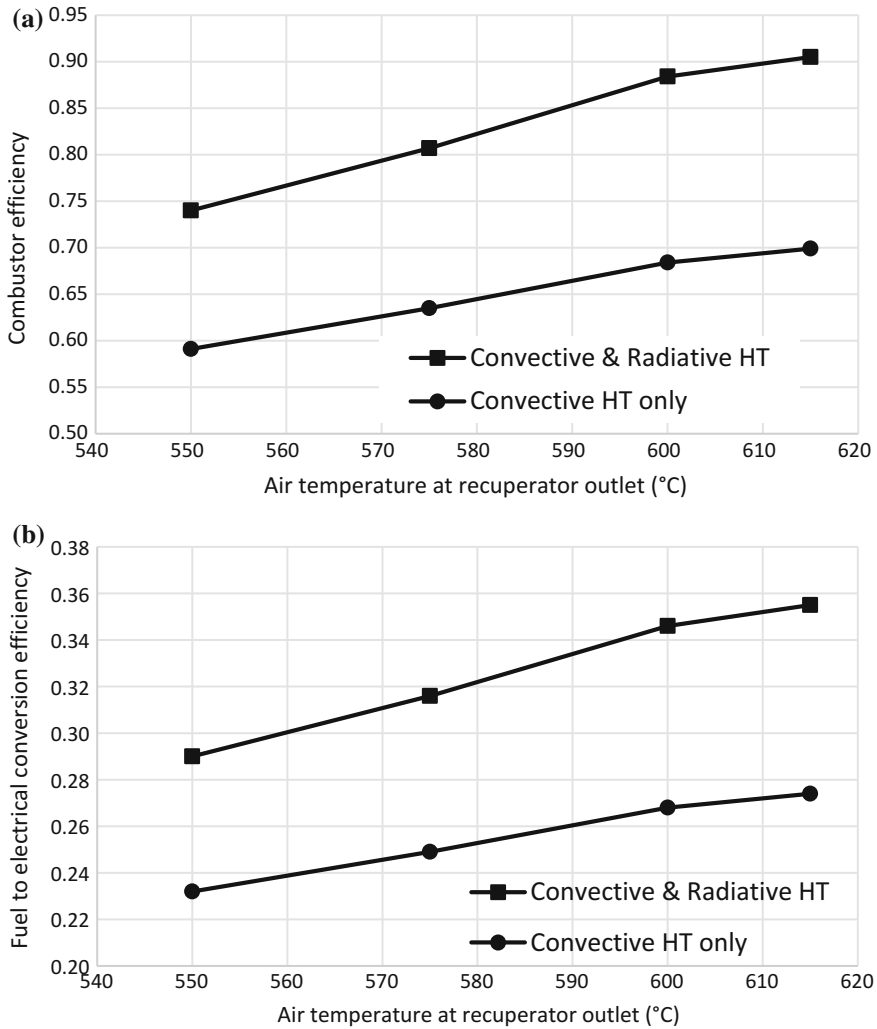


Fig. 14.13 Sensitivity with respect to recuperator air outlet temperature for **a** combustor efficiency and **b** fuel-to-electrical conversion efficiency

Fig. 14.16a (due to reduced ΔT between the burned fuel temperature and heater head temperature). The black dashed line with open symbols in Fig. 14.16a shows the Stirling engine heat to electrical conversion efficiency, which increases with an increase in heater head temperature. This is expected as the Carnot efficiency is expected to increase with an increase in the heater head temperature (see Eq. 14.9). The 700 °C point therefore represents an inflection point where the reduction in combustor efficiency can be compensated by the increase in the Carnot efficiency of the engine. Beyond this point, any increase in Carnot efficiency is not sufficient to

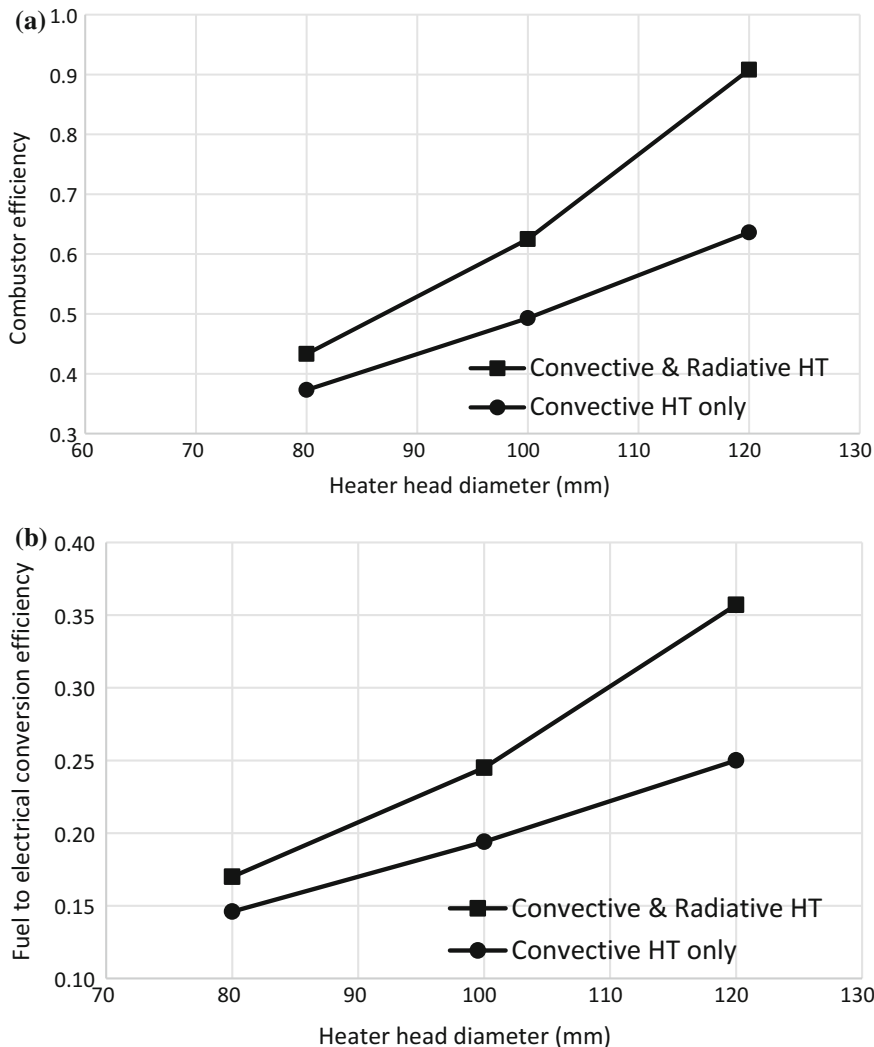


Fig. 14.14 Sensitivity with respect to heater head diameter for **a** combustor efficiency and **b** fuel-to-electrical conversion efficiency

overcome the loss in the combustor efficiency. Note that for the scenarios in Fig. 14.16, the air temperature at the recuperator outlet was maintained fairly constant and limited to 575 °C (due to material limits), which lead to higher exhaust temperatures for scenarios with heater head temperatures greater than 700 °C. Thus, this results in lower combustor efficiencies for scenarios with heater head temperatures greater than 700 °C when compared to scenarios with heater head temperatures lower than 700 °C. Thus, the design of a combustion-driven Stirling engine

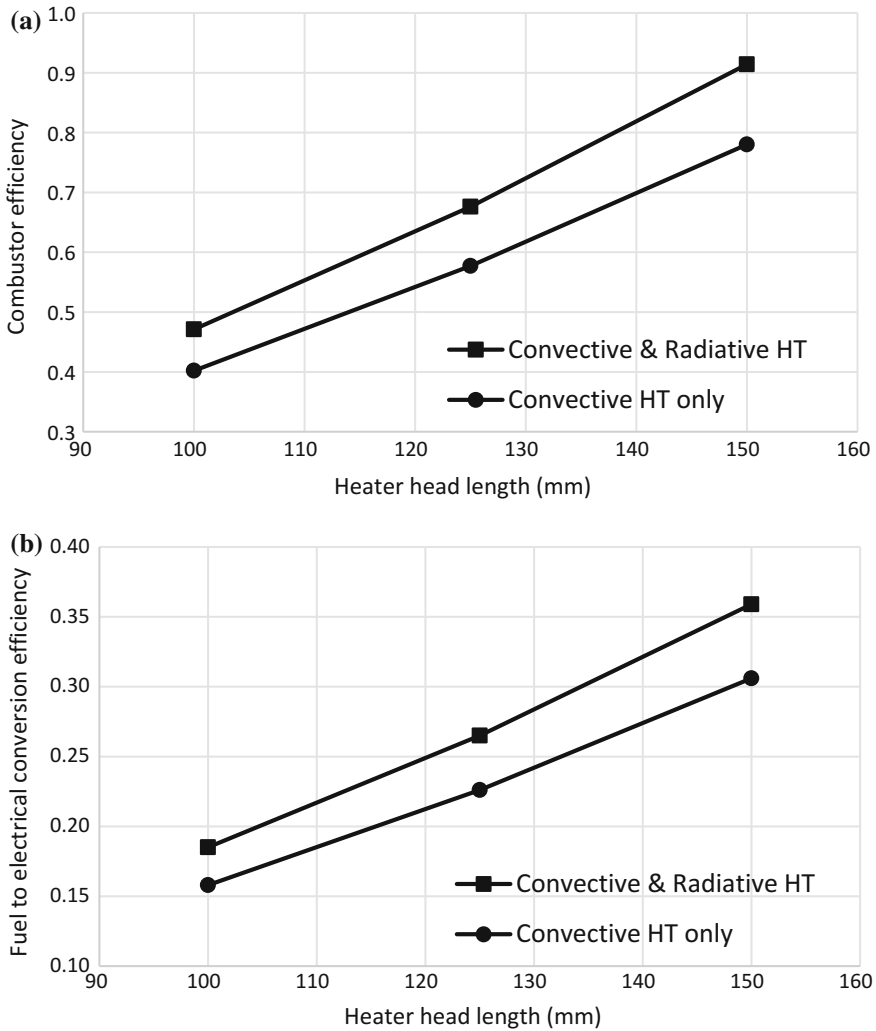


Fig. 14.15 Sensitivity with respect to heater head length for **a** combustor efficiency and **b** fuel-to-electrical conversion efficiency

is extremely challenging and a rigorous system-level approach, which must include the co-optimization of the combustion system and the Stirling engine (rather than individual component optimization), is necessary. Radiative heat transfer is also critical for achieving a high combustor and engine efficiency for dome-shaped heater head Stirling engines.

Li et al. (2014) published a modeling study of a high-efficiency Stirling engine that showed a potential to achieve 43.9% indicated thermal efficiency while delivering a low indicated power of 33.4 W (1.88 W/cm³). The system takes

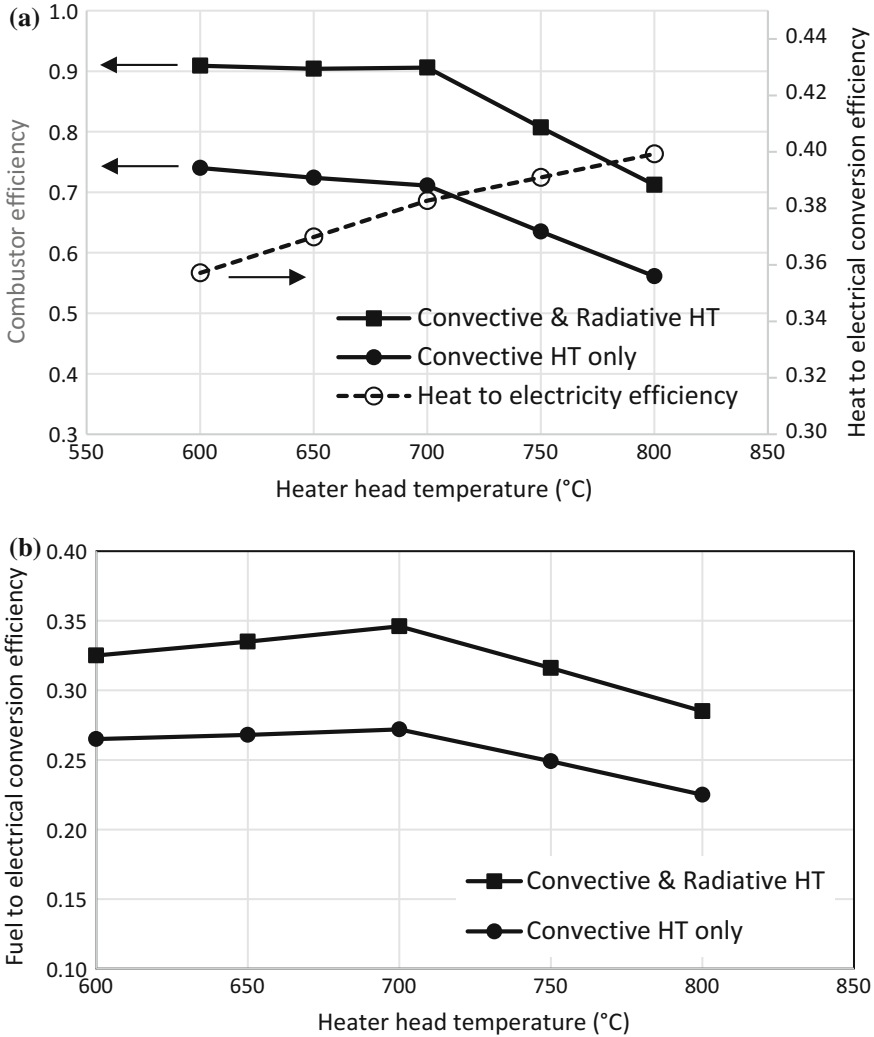


Fig. 14.16 Sensitivity with respect to heater head wall temperature for **a** combustor efficiency and **b** fuel-to-electrical conversion efficiency

advantage of a compact porous sheet heat exchanger, which incorporates the heater, regenerator, and cooler into one assembly; the hypothesis for this approach was that a significant reduction in friction could be achieved with such a system. The major benefits of using micro-channels include reduction in flow separation and formation of wakes, low surface roughness, lower flow velocities, and lower conduction heat losses. However, this requires radical improvements in emerging micro-fabrication technologies for mass production of such heat exchangers.

Recent efforts have focused on fabricating Stirling engine components by additive manufacturing (AM) in order to increase efficiency. This is a powerful manufacturing process that can yield complex and intricate geometries, not possible by traditional manufacturing methods. In addition to increasing the effectiveness of the heat exchange process, the interfacial heat transfer losses, e.g. between the burner and the heat acceptor interface, are also projected to be minimized by additively manufacturing a single unit without using conventional joining techniques. As reported by Zelinski in *Additive Manufacturing Magazine* (*Additive Manufacturing* 2015), DEKA Research and Development is currently investigating the use of additively manufactured components, e.g. burner and Stirling engine heater head, to improve engine efficiency. Figure 14.17a, reprinted from *Additive Manufacturing* (2015), shows the additively manufactured heater head from Inconel 625 material (Stirling engine heater head on the left), which is traditionally used for high-temperature applications. DEKA is also working on additively manufacturing heater heads with Mar-M-247, which is superior in retaining high-temperature strength as compared to Inconel 625. Figure 14.17a shows also the conventional

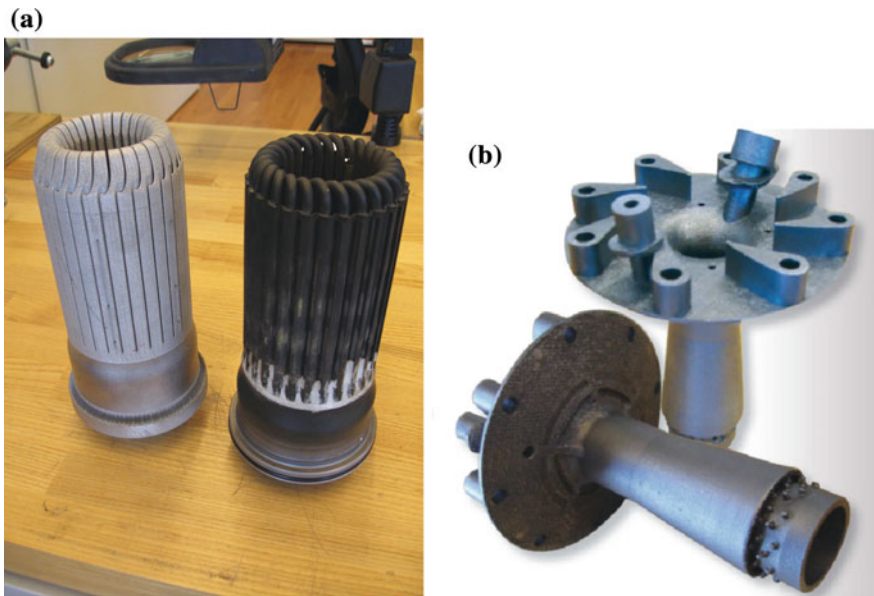


Fig. 14.17 **a** Additively manufactured Stirling engine heater head (left) and conventional tubular heater head (right) and **b** additively manufactured Stirling engine burner (*Additive Manufacturing* 2015) manufactured by DEKA Research and Development. Originally appeared in *Additive Manufacturing Magazine*, copyright 2015 Gardner Business Media, Inc. Used with permission

heater head (on the right) which has tubes to carry the working fluid (e.g. helium) that are bent and welded at numerous places. This heater head design is called the tubular heater head. The custom shape of the fluid passages in the additively manufactured heater head is expected to better capture the heat of combustion than the conventional version of the heater head. The burner sits at the center of the heater head transferring heat to the working fluid that flows inside the tubes. One of the well-known traditional disadvantages of AM is the resulting surface roughness of the end product. As surface roughness accelerates the transition from laminar to turbulent flow, the heat transfer to the working fluid inside the tubes is also expected to be improved (Additive Manufacturing 2015). Figure 14.17b, reprinted from Additive Manufacturing (2015), shows an additively manufactured Stirling engine burner throat, where the tear-drop flanges help in fuel–air mixing, while the spout end of the burner holds a stable flame at the center of the heater head.

Song et al. (2015) achieved better heat transfer in a tubular heater head Stirling engine, similar to the one shown in Fig. 14.17a, by employing steel wool into the space between the outside of the tubes for recuperating exhaust gas energy. As expected, the steel wool resulted in increased surface area for heat transfer. In addition, the steel wool had a higher emissivity than the exhaust gas, which resulted in enhanced heat transfer between the exhaust gases and the outer surface of the tubes. The porosity of the steel wool was varied in their experiments, and it was found that the convection heat transfer coefficient (h) increased with decreasing porosity at a constant exhaust gas velocity. However, in a typical NG-fired Stirling engine, the additional pressure drop created by the low porosity steel wool can result in higher parasitic power for the fuel and air blowers. Thus, a tradeoff in the system efficiency is expected, which will be governed primarily by improved heat transfer and a concomitant increase in parasitic power. More recently, a detailed summary of the technical challenges of Stirling engine systems has been published by Hachem et al. (2018).

Sunpower, Inc. (Athens, Ohio, USA), in collaboration with Aerojet Rocketdyne and Precision Combustion, Inc. has developed a free-piston Stirling engine (FPSE) with a recuperated two-stage catalytic combustor under the ARPA-E GENSETS program (Wood 2018). As of early 2018, the engine demonstrated a fuel-to-electrical conversion efficiency of 20.5% with a peak heat to electrical conversion efficiency of 38.8% and a peak combustor efficiency of 64%. The output power of the engine is lower than 1 kW. Further improvements in recuperator sizing and recuperator heat loss reduction are required to improve the system efficiency. Figure 14.18 shows the assembled prototype Stirling engine system (Wood 2018) that was developed by Sunpower, Inc. under the ARPA-E GENSETS program.

West Virginia University Research Corporation (WVURC) located in Morgantown, West Virginia, USA, is currently developing an additively manufactured Stirling engine heater head design under the ARPA-E GENSETS program (Qiu 2018). A computational study of the heat transfer in a stainless steel Stirling engine heater head was recently published by this team (Solomon and Qiu 2018).

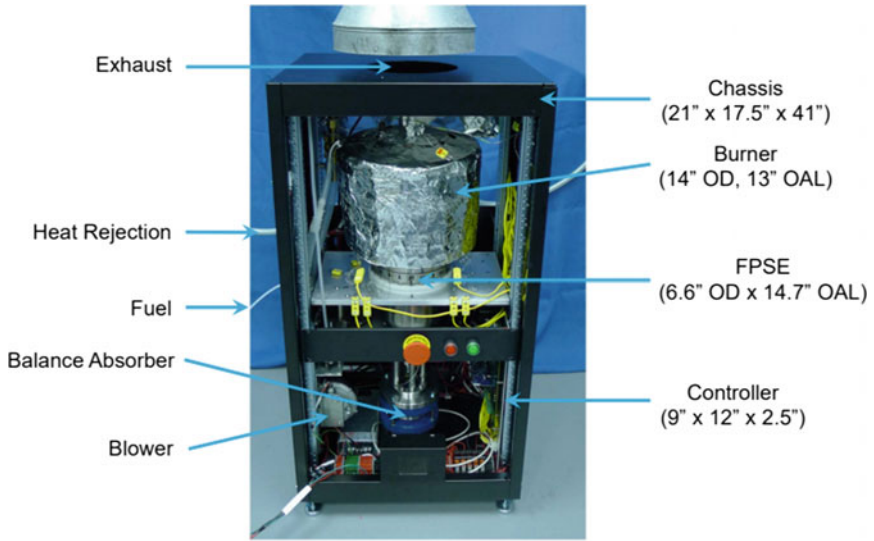


Fig. 14.18 Prototype Stirling engine system developed by Sunpower, Inc. (Wood 2018)

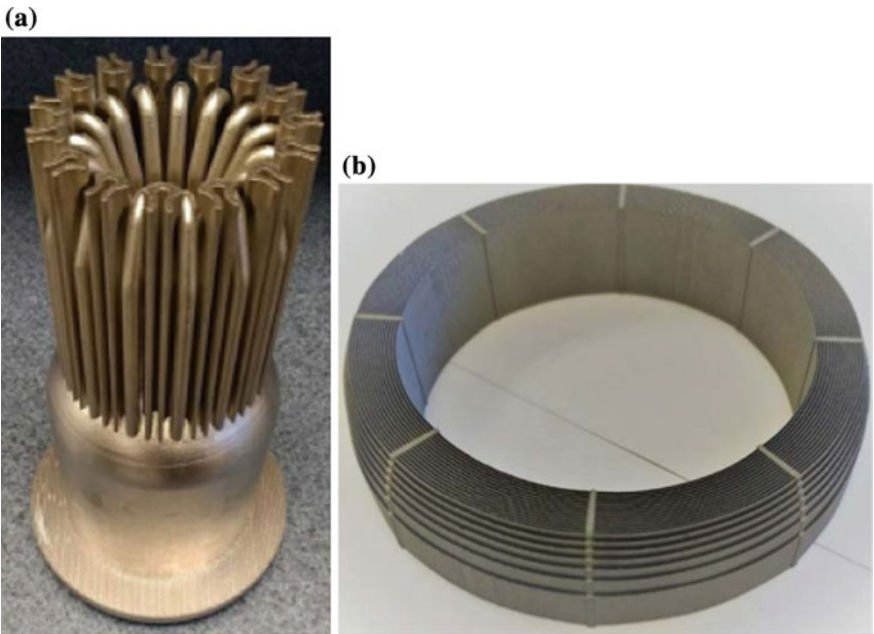


Fig. 14.19 a Image of the additively manufactured Stirling engine heater head design and b additively manufactured involute foil regenerator developed by West Virginia University (Qiu 2018)

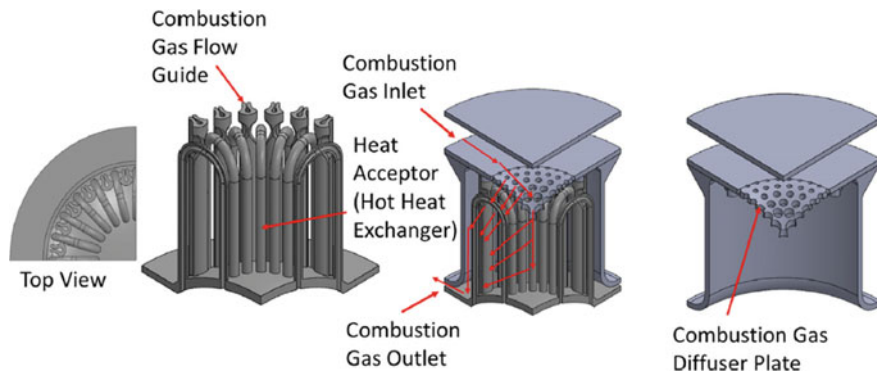


Fig. 14.20 Flow path of the exhaust gas through the additively manufactured heater head design developed by West Virginia University (Solomon and Qiu 2018)

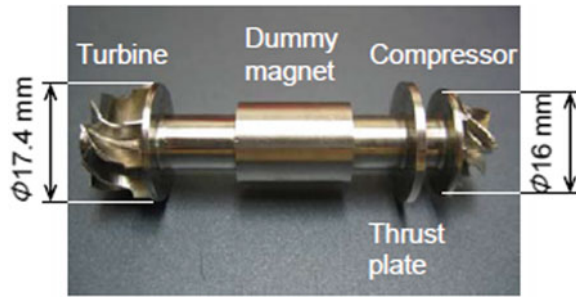
Figure 14.19a, reprinted from Qiu (2018), shows the additively manufactured heater head design, and Fig. 14.19b, reprinted from Qiu (2018), shows the additively manufactured involute foil regenerator (the regenerator is an internal heat exchanger in a Stirling engine, which stores thermal energy from the working fluid that would otherwise be rejected at the cold end of the engine and supplies that energy back to the working fluid in the next thermodynamic cycle when the working fluid shuttles to the hot end of the engine). Both designs are expected to improve the Stirling engine fuel-to-electrical conversion efficiency. Figure 14.20, reprinted from Solomon and Qiu (2018), shows the flow path of the combustion gas in the Stirling engine heater head. The combustion gas guides are provided for improving heat transfer with the tubes. The vented diffuser plate was used to provide uniform distribution of the hot combustion gas over the tubular heat exchanger.

14.3.3 Brayton Cycle Engines

It is more challenging for Brayton cycle engines, particularly with conventional radial turbomachinery, to be efficient at small scales due to significant flow and heat transfer losses. At the 1–10 kW scale, Brayton engines are arguably less mature than ICEs and Stirling engines.

McDonald and Rogers (2008) investigated the use of a ceramic micro-turbine concept with a ceramic combustor, ceramic radial flow turbine, and a ceramic (silicon carbide) high-effectiveness recuperator. Projected efficiency for such a system was 30% while delivering a peak power of 7.5 kW. Tanaka et al. (2007) tested what they claimed as the world's smallest turbine operating on a Brayton cycle. The engine comprised of a compressor with an impeller diameter of 16 mm, a turbine with a diameter of 17.4 mm, an annular swirl flow combustor, and a

Fig. 14.21 World's smallest micro-turbine Brayton cycle engine reprinted from the work of Tanaka et al. (2007)



dummy electromagnetic generator. The rotor was supported with pressurized gas bearings. An image of this turbine hardware is shown in Fig. 14.21, which is reprinted from their work. The compressor was seen to approach the design adiabatic efficiency at 55% and 70% of the rated speed (580,000 rpm).

Under the ARPA-E GENSETS program, Brayton Energy, LLC (Hampton, New Hampshire, USA), is developing a rotary screw Brayton cycle engine with metallic screw compressors and ceramic screw expanders. Screw components do not suffer from flow losses that are present in conventional radial turbomachinery. In addition, the use of a ceramic expander with low coefficient of thermal expansion can lead to high-temperature tolerance and a better fuel-to-electrical conversion efficiency due to higher Carnot efficiency. A highly recuperated combustor will be used in this project. As of early 2018, Brayton Energy has demonstrated a 75% isentropic efficiency for the compressor when operated with a rotor clearance of 68μ (Kesseli et al. 2018). Figure 14.22a, b shows the coated screw compressor and ceramic rotary screw expander, respectively, developed by Brayton Energy under the ARPA-E GENSETS program (Kesseli 2018; Kesseli et al. 2018).

Metis Design Corporation (MDC), located in San Francisco, California, USA, in collaboration with Lawrence Berkeley National Laboratory (LBNL), Brayton Energy, LLC, and University of Texas—Arlington is developing a 1-kW micro-turbine with a compressor and a rotary vaneless diffuser (RVD) under the GENSETS program. The RVD rotates at a much lower speed compared to the compressor impeller and reduces the kinetic energy losses of the flow that exits at a high speed from the impeller. A recuperated low swirl burner is intended to be integrated with the micro-turbine. Figure 14.23 shows the compressor hardware with the impeller and the RVD (Keogh et al. 2018). As of early 2018, the team has demonstrated approximately 75% isentropic efficiency for the compressor at 50% of the impeller design speed (Keogh et al. 2018).

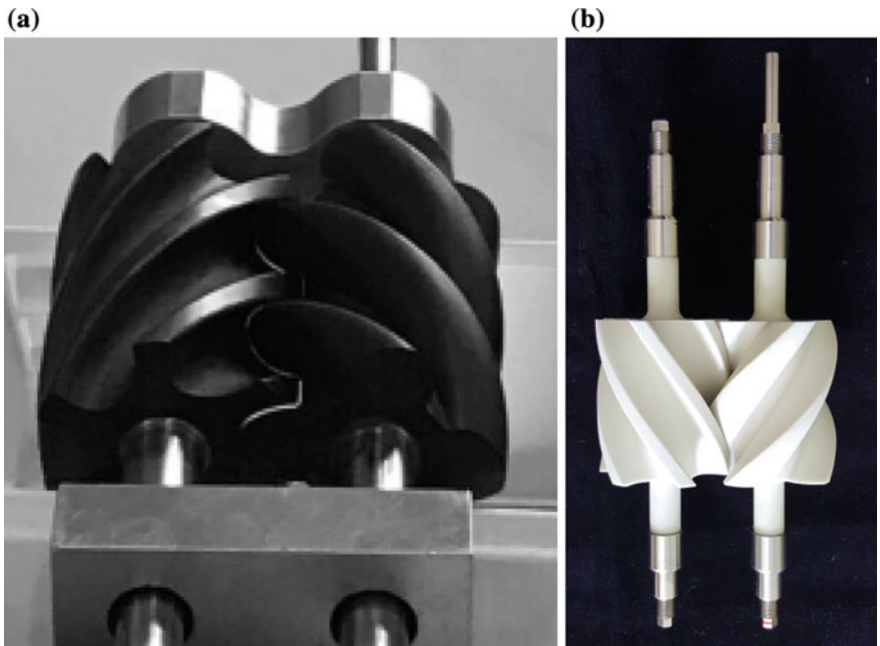


Fig. 14.22 **a** Coated screw compressor (Kesseli et al. 2018) and **b** ceramic rotary screw expander (Kesseli 2018) as developed by Brayton Energy

Fig. 14.23 Micro-turbine impeller and RVD as developed by MDC (Keogh et al. 2018)



14.4 Summary

This chapter presented a detailed review of the state-of-the-art residential CHP technologies encompassing reciprocating internal combustion engines (ICEs), Stirling engines, Brayton cycle engines, and micro-Rankine cycle engines. This was complemented by anecdotal highlights from some of the cutting-edge technologies funded by Advanced Research Projects Agency-Energy (ARPA-E). From a fuel conversion efficiency and load-following standpoint, reciprocating ICEs are considered to have the most benefits, but have some disadvantages such as regular maintenance (oil change, part replacement, etc.). Heat transfer, incomplete combustion, pumping, and friction losses at the small scale are found to be the technical hurdles for ICEs. Thus, technologies such as spark-assisted homogeneous charge compression ignition (SA-HCCI), turbulent jet ignition (TJI), and low-friction components are identified as potential enabling approaches for improving fuel conversion efficiency. Additionally, Stirling engines and Brayton cycle engines offer excellent fuel flexibility and hence are more resistant to the quality of NG as compared to ICEs.

Stirling engines have demonstrated lower fuel conversion efficiency compared to ICEs, but they can operate without maintenance for a significant amount of time. One of the biggest hurdles for improving Stirling engine fuel conversion efficiency is to achieve effective heat transfer between the combusting fuel and the working fluid of the engine. Radiation heat transfer and a high degree of intake air recuperation are found to be key mechanisms for enhancing heat transfer in dome-shaped Stirling engines. Additive manufacturing is considered to be one of the key enablers for improving tubular heater head Stirling engine efficiency by enhancing heat transfer through unique designs that are complex to fabricate by conventional manufacturing processes. Irrespective of the Stirling engine heater head design, a co-optimization of the combustion system and the Stirling engine is necessary for improving their fuel conversion efficiency.

Brayton cycle machines are the least mature technology at the 1–10 kW size as evidenced by the availability of just one commercial 3-kW micro-turbine product. Brayton cycle engines have also demonstrated lower efficiencies compared to ICEs. Challenges include achieving high compressor and expander isentropic efficiencies at the small power level.

Finally, the most important driver for customer adoption is the total installed cost of the micro-CHP system (Vishwanathan et al. 2018) and the system must be simple to install and maintain.

References

- Additive Manufacturing—Aug 2015, <https://am.epubxp.com/i/542042-aug-2015/6>. Last Accessed 26 July 2018
- Aisin 1.5 kW internal combustion engine CHP. ARPA-E GENSETS Annual Program Review Meeting, Denver, CO, U.S (2016). URL: https://arpa-e.energy.gov/sites/default/files/Sekihisa_Aisin.pdf

- Ashurst S (2016) Insights on the global micro-CHP market. ARPA-E GENSETS Annual Review Meeting, Denver, CO, U.S. URL: https://arpa-e.energy.gov/sites/default/files/Ashurst_DeltaEE.pdf
- Ashurst S (2018) E-mail Communication, 12 March 2018
- Barbieri ES, Spina PR, Venturini M (2012) Analysis of innovative micro-CHP systems to meet household energy demands. *Appl Energy* 97:723–733. <https://doi.org/10.1016/j.apenergy.2011.11.081>
- Baukal CE, Gebhart B (1996) A review of empirical flame impingement heat transfer correlations. *Int J Heat Fluid Flow* 17:386–396. [https://doi.org/10.1016/0142-727X\(96\)00003-3](https://doi.org/10.1016/0142-727X(96)00003-3)
- Bunce M (2018) Advanced lean burn micro-CHP GENSET. GENSETS Annual Program Review Meeting, Washington, DC, U.S. URL: https://arpa-e.energy.gov/sites/default/files/8_Bunce-MPT_GENSETS_Annual_Review_3-2018.pdf
- Capaldi P (2014) A high efficiency 10 kW microcogenerator based on an Atkinson cycle internal combustion engine. *Appl Therm Eng* 71:913–920. <https://doi.org/10.1016/j.applthermaleng.2014.02.035>
- Carbon Flow Charts, <https://flowcharts.llnl.gov/commodities/carbon>. Last Accessed 14 July 2018
- Caton JA (2014) On the importance of specific heats as regards efficiency increases for highly dilute IC engines. *Energy Convers Manage* 79:146–160. <https://doi.org/10.1016/j.enconman.2013.12.020>
- Cheng W, Wong V, Plumley M, Martins T, Molewyk M, Gu G, Park S-Y (2014) Lubricant formulations to enhance engine efficiency in modern internal combustion engines, 2014 annual merit review, vehicle technologies office. U.S. Department of Energy, Washington, DC, U.S. Climate Zones|Department of Energy, <https://www.energy.gov/eere/buildings/climate-zones>. Last Accessed 15 July 2018
- CP5WN Model CP5WN CP5WN-SNB CP5WN-SPB, <http://www.yanmar-es.com/wp-content/uploads/CP5WN-Spec-Sheet.pdf>. Last Accessed 16 July 2018
- CP10WN, <http://www.yanmar-es.com/wp-content/uploads/CP10WN-Spec-Sheet.pdf>. Last Accessed 16 July 2018
- Cullen B, McGovern J (2010) Energy system feasibility study of an Otto cycle/Stirling cycle hybrid automotive engine. *Energy* 35:1017–1023. <https://doi.org/10.1016/j.energy.2009.06.025>
- Dec JE (2009) Advanced compression-ignition engines—understanding the in-cylinder processes. *Proc Combust Inst* 32:2727–2742. <https://doi.org/10.1016/J.PROCI.2008.08.008>
- De Paepe M, D’Herdt P, Mertens D (2006) Micro-CHP systems for residential applications. *Energy Convers Manage* 47:3435–3446. <https://doi.org/10.1016/j.enconman.2005.12.024>
- EIA recs, <https://www.eia.gov/consumption/residential/data/2015/hc/php/hc1.1.php>. Last Accessed 14 July 2018
- Energy Flow Charts, <https://flowcharts.llnl.gov/>. Last Accessed 14 July 2018
- Ferreira AC, Nunes ML, Teixeira JCF, Martins LASB, Teixeira SFCF (2016) Thermodynamic and economic optimization of a solar-powered stirling engine for micro-cogeneration purposes. *Energy* 111:1–17. <https://doi.org/10.1016/J.ENERGY.2016.05.091>
- Fontana G, Galloni E (2009) Variable valve timing for fuel economy improvement in a small spark-ignition engine. *Appl Energy* 86:96–105. <https://doi.org/10.1016/j.apenergy.2008.04.009>
- Fubara TC, Cecelja F, Yang A (2014) Modelling and selection of micro-CHP systems for domestic energy supply: the dimension of network-wide primary energy consumption. *Appl Energy*. <https://doi.org/10.1016/j.apenergy.2013.09.069>
- Gangopadhyay A, Mcwatt DG, Zdrodowski RJ (2012) Engine friction reduction through surface finish and coatings. In: Conference on directions in engine efficiency and emissions research (DEER), Dearborn, MI, U.S. URL: https://www1.eere.energy.gov/vehiclesandfuels/pdfs/deer_2012/friday/presentations/deer12_gangopadhyay.pdf
- García D, González MA, Prieto JI, Herrero S, López S, Mesonero I, Villasante C (2014) Characterization of the power and efficiency of stirling engine subsystems. *Appl Energy* 121:51–63. <https://doi.org/10.1016/j.apenergy.2014.01.067>

- GENSETS, <https://arpa-e.energy.gov/?q=arpa-e-programs/gensets>. Last Accessed 21 July 2018
- Goto S, Moriya K, Kosaka H, Akita T, Hotta Y, Umeno T, Nakakita K (2014) Development of free piston engine linear generator system Part 2—investigation of control system for generator. SAE technical paper 2014-01-1193. <https://doi.org/10.4271/2014-01-1193>
- Guyer E (2015) First-hand experience with residential micro-CHP in the United States: status and challenges. ARPA-E GENSETS Program Kickoff Meeting, Chicago, IL, U.S. URL: https://arpa-e.energy.gov/sites/default/files/Guyer_YankeeScientific_GENSETS.pdf
- Guyer E (2016) Micro-CHP demonstration planning. A report prepared for U.S. Department of Energy, ARPA-E
- Hachem H, Gheith R, Aloui F, Ben Nasrallah S (2018) Technological challenges and optimization efforts of the stirling machine: a review. *Energy Convers Manag* 171:1365–1387. <https://doi.org/10.1016/J.ENCONMAN.2018.06.042>
- Honda Worldwide|Power products—household gas engine cogeneration unit, <http://world.honda.com/power/cogenerator/>. Last Accessed 14 July 2018
- <https://www.mtrigen.com/>, Last Accessed 11 Aug 2018
- Incropera FP, DeWitt DP (2002) *Fundamentals of heat and mass transfer*, 5th edn. Wiley, Hoboken, NJ, U.S.
- Keller BP, Nelson SE, Walton KL, Ghosh TK, Tompson RV, Loyalka SK (2015) Total hemispherical emissivity of Inconel 718. *Nucl Eng Des* 287:11–18. <https://doi.org/10.1016/j.nucengdes.2015.02.018>
- Keogh R, Kesseli J, Therkelsen P, Kim D (2018) 1 kW microturbine system. GENSETS Annual Program Review Meeting, Washington, DC, U.S. URL: https://arpa-e.energy.gov/sites/default/files/6_GENSETS_workshop_2018_RCK_v5.pdf
- Kesseli J (2018) E-mail Communication, 27 July 2018
- Kesseli J, Everbeck C, Wolf T (2018) Recuperated brayton cycle engine using a screw compressor and expander. GENSETS Annual Program Review Meeting, Washington, DC, U.S. URL: https://arpa-e.energy.gov/sites/default/files/5_GENSETS-2018-03-12_BRAYTON-Rev-3.pdf
- Killingsworth NJ, Rapp VH, Flowers DL, Aceves SM, Chen JY, Dibble R (2011) Increased efficiency in SI engine with air replaced by oxygen in argon mixture. *Proc Combust Inst* 33:3141–3149. <https://doi.org/10.1016/j.proci.2010.07.035>
- Kobayashi K, Sako T, Sakaguchi Y, Morimoto S, Kanematsu S, Suzuki K, Nakazono T, Ohtsubo H (2011) Development of HCCI natural gas engines. *J Nat Gas Sci Eng* 3:651–656. <https://doi.org/10.1016/j.jngse.2011.07.002>
- Koga H, Kiura T (2013) A study of controlled auto-ignition in small natural gas engines. *SAE Int J Engines* 6:2133–2139
- Kosaka H, Akita T, Moriya K, Goto S, Hotta Y, Umeno T, Nakakita K (2014) Development of free piston engine linear generator system Part 1—Investigation of fundamental characteristics. SAE technical paper 2014-01-1203. <https://doi.org/10.4271/2014-01-1203>
- Li Z, Haramura Y, Kato Y, Tang D (2014) Analysis of a high performance model stirling engine with compact porous-sheets heat exchangers. *Energy* 64:31–43. <https://doi.org/10.1016/j.energy.2013.11.041>
- Maghanki MM, Ghobadian B, Najafi G, Galogah RJ (2013) Micro combined heat and power (MCHP) technologies and applications. *Renew Sustain Energy Rev* 28:510–524. <https://doi.org/10.1016/j.rser.2013.07.053>
- MAZDA: Next-generation technology, <http://www2.mazda.com/en/next-generation/technology/>. Last Accessed 01 Aug 2018
- McDonald CF, Rodgers C (2008) Small recuperated ceramic microturbine demonstrator concept. *Appl Therm Eng* 28:60–74. <https://doi.org/10.1016/j.applthermaleng.2007.01.020>
- Micro CHP products, http://micro-chp.com/micro_chp_products.htm
- MTT EnerTwin, https://www.enertwin.com/cms/EN_Specifications_EnerTwin-2017.pdf. Last Accessed 20 July 2018
- Muccillo M, Gimelli A (2014) Experimental development, 1D CFD simulation and energetic analysis of a 15 kw micro-CHP unit based on reciprocating internal combustion engine. *Appl Therm Eng* 71:760–770. <https://doi.org/10.1016/j.applthermaleng.2013.11.025>

- Parlak A, Yasar H, Eldogan O (2005) The effect of thermal barrier coating on a turbo-charged diesel engine performance and exergy potential of the exhaust gas. *Energy Convers Manage* 46:489–499. <https://doi.org/10.1016/j.enconman.2004.03.006>
- Qiu S (2018) Advanced stirling power generation systems for combined heat and power (ASPGen). GENSETS Annual Program Review Meeting, Washington, DC, U.S. URL: https://arpa-e.energy.gov/sites/default/files/3_GENSETS%20annual%20review%20meeting%20WVU%20Stirling%20S.pdf
- Qnergy SmartBoiler, <https://www.qnergy.com/wp-content/uploads/2018/01/Download-the-SmartBoiler-Brochure-Spec-Sheet.pdf>. Last Accessed 16 July 2018
- Reitz R, Wickman D, Wright C, Kokjohn S, Andrie M, Shears D, Procknow D, Kamo L (2018) Spark-assisted HCCI residential CHP. GENSETS Annual Program Review Meeting, Washington, DC, U.S. URL: https://arpa-e.energy.gov/sites/default/files/9_GENSETS%20-%20WERC-Final.pdf
- Ren H, Gao W (2010) Economic and environmental evaluation of micro CHP systems with different operating modes for residential buildings in Japan. *Energy Build* 42:853–861. <https://doi.org/10.1016/J.ENBUILD.2009.12.007>
- Sevier DK (2015) Oil & gas industry electric power for upstream operations. ARPA-E GENSETS Program Kickoff Meeting, Chicago, IL, U.S. URL: https://arpa-e.energy.gov/sites/default/files/Sevier_SWN_GENSETS.pdf
- Sherman RA (1934) Radiation from luminous and non-luminous natural gas flames. *Trans ASME* 56:177–192
- Solomon L, Qiu S (2018) Computational analysis of external heat transfer for a tubular stirling convertor. *Appl Therm Eng* 137:134–141. <https://doi.org/10.1016/J.APPLTHERMALENG.2018.03.070>
- Song Z, Chen J, Yang L (2015) Heat transfer enhancement in tubular heater of stirling engine for waste heat recovery from flue gas using steel wool. *Appl Therm Eng* 87:499–504. <https://doi.org/10.1016/J.APPLTHERMALENG.2015.05.028>
- Taie Z, West B, Szybist J, Edwards D, Thomas J, Huff S, Vishwanathan G, Hagen C (2018) Detailed thermodynamic investigation of an ICE-driven, natural gas-fueled, 1 kW micro-CHP generator. *Energy Convers Manag* 166. <https://doi.org/10.1016/j.enconman.2018.04.077>
- Tanaka S, Hikichi K, Togo S, Murayama M, Hirose Y, Sakurai T, Yuasa S, Teramoto S, Niino T, Mori T et al (2007) World's smallest gas turbine establishing Brayton cycle. *Tech Dig PowerMEMS* 2007:359–362
- Tapia-Ahumada K, Pérez-Arriaga IJ, Moniz EJ (2013) A methodology for understanding the impacts of large-scale penetration of micro-combined heat and power. *Energy Policy* 61:496–512. <https://doi.org/10.1016/j.enpol.2013.06.010>
- Taylor CF (1985) *The internal-combustion engine in theory and practice: Volume 1: Thermodynamics, fluid flow, performance*, 2nd edn. MIT press, Cambridge, Massachusetts, U.S
- Valenti G, Silva P, Fergnani N, Di Marcoberardino G, Campanari S, Macchi E (2014) Experimental and numerical study of a micro-cogeneration Stirling engine for residential applications. *Energy Procedia* 45:1235–1244
- Vishwanathan G, Sculley JP, Fischer A, Zhao J-C (2018) Techno-economic analysis of high-efficiency natural-gas generators for residential combined heat and power. *Appl Energy* 226:1064–1075
- Visser WPJ, Shakariyants SA, Oostveen M (2011) Development of a 3 kW microturbine for CHP applications. *J Eng Gas Turbines Power* 133:042301. <https://doi.org/10.1115/1.4002156>
- Visser WPJ, Shakariyants S, de Later MTL, Ayed AH, Kusterer K (2012) Performance optimization of a 3 kW microgasturbine for CHP applications. In: *Proceedings of ASME Turbo Expo 2012: turbine technical conference and exposition*, pp 619–628. American Society of Mechanical Engineers, Copenhagen, Denmark
- Wood G (2018) Free piston stirling engine based 1 kW generator. GENSETS Annual Program Review Meeting, Washington, DC, U.S. URL: https://arpa-e.energy.gov/sites/default/files/1_Sunpower_2018-03-19_GENSETS_Year_2_review_final.pdf
- Yanmar mCHP, <http://www.yanmar-es.com/wp-content/uploads/YANMAR-mCHP-Catalog-2016-Update.pdf>. Last Accessed 20 July 2018